Weather Type Reconstruction using Machine Learning Approaches

Lucas Pfister[1,2], Lena Wilhelm[1,2], Yuri Brugnara*[1,2], Noemi Imfeld[1,2], and Stefan Brönnimann [1,2]

[1]Oeschger Centre for Climate Change Research, University of Bern, Bern, 3012, Switzerland
[2]Institute of Geography, University of Bern, Bern, 3012, Switzerland
*now at Empa, Dübendorf, 8600, Switzerland

Correspondence: Lucas Pfister (lucas.pfister@unibe.ch)

Abstract. Weather types are used to characterise large–scale synoptic weather patterns over a region. Long–standing records of weather types hold important information about day–to–day variability and changes of atmospheric circulation and the associated effects on the surface. However, most weather type reconstructions are restricted in their temporal extent and suffer from methodological limitations. In our study, we assess various machine learning approaches for station–based weather type reconstruction over Europe based on the nine-class "cluster analysis of principal components" (CAP9) weather type classification. With a common feedforward neural network performing best in this model comparison, we reconstruct a daily CAP9 weather type series back to 1728. This new reconstruction constitutes the longest daily weather type series available. A detailed validation shows considerably better performance compared to previous statistical approaches and good agreement with the reference series for various climatological analyses. Our approach may serve as a guide for other weather type classifications.

1 Introduction

Weather type (WT) or circulation type classifications are a widespread tool to characterize the prevailing large–scale synoptic weather patterns over a specific region (Philipp et al., 2010). In regions such as Europe, where daily weather is largely governed by transient high and low pressure systems, such classifications prove particularly useful to describe the prevailing atmospheric conditions. WT time series yield important information about variability and changes of atmospheric patterns (Jones et al., 2014; Rohrer et al., 2017; Kučerová et al., 2017) and the surface effects associated with them (Paegle, 1974; O'Hare and Sweeney, 1993; Kostopoulou and Jones, 2007; Lorenzo et al., 2008; Jones and Lister, 2009; Casado et al., 2010; Küttel et al., 2011). Various studies have assessed the links between WTs and extreme events such as droughts (Fleig et al., 2010), temperature extremes (Hoy et al., 2020; Sýkorová and Huth, 2020) or extreme precipitation and floods (Minářová et al., 2017; Petrow et al., 2009). Moreover, WT classifications are applied for evaluating weather forecast model outputs (Stryhal and Huth, 2019; Weusthoff, 2011) or forecasting in the renewable energy sector (Wang et al., 2022; Drücke et al., 2021; Li et al., 2020), among others.

The first WT classifications were created by experienced meteorologists who classified the atmospheric situation employing manually drawn weather charts derived from station observations (Hess and Brezowsky, 1952; Lamb, 1972; Schüepp, 1979). While these subjective classifications represent real synoptic features, they are often subject to inconsistencies and ambiguities

(e.g. James, 2007; Cahynová and Huth, 2009; Jones et al., 2014; Wanner et al., 2000). In more recent decades, hybrid (mixed) or objective (automatized) WT classifications have been introduced that classify atmospheric patterns numerically using various statistical approaches, such as clustering algorithms, class attribution based on a distance measure, or even machine learning approaches (Huth et al., 2008; Mittermeier et al., 2022). Such automatized WT classification is usually based on gridded meteorological data (Huth et al., 2008). Because the temporal coverage of such gridded datasets is limited, WT classifications usually only reach back several decades. By creating long–term time-series of WT classifications, important information may be gained to study long–term changes (i.e. over multiple decades or even centuries) in atmospheric circulation patterns and associated surface effects.

Based on reanalysis datasets, many WT records could already be extended back to the 19th century (Philipp et al., 2010; Jones et al., 2014). The latest generation of reanalyses would allow these to be extended even further back in time. Currently, the limit for WT classifications based on atmospheric fields is set by the 20th Century Reanalysis version 3 (20CRv3; Slivinski et al., 2019; Compo et al., 2011), which extends back to 1806. Prior to that, historical station observations and qualitative descriptions of the atmospheric conditions from weather diaries are the only sources available for classifying WTs. This data, however, is vital to study the past development of atmospheric processes on a daily to sub-daily scale far beyond the availability of reanalyses, as can be done by creating station-based WT reconstructions. Recent data rescue and digitisation efforts (Brunet and Jones, 2011; Brönnimann et al., 2019; Pfister et al., 2019; Brugnara et al., 2019, 2020b, 2022b) brought to light a vast amount of early instrumental meteorological records which can be used for this purpose, particularly in central Europe. Only a small number of studies have used this data so far, resulting in some long–term, station–based WT reconstructions starting in the middle of the 18th century (Schwander et al., 2017; Delaygue et al., 2019). Despite that station observations as point measurements hold only limited information on the circulation patterns over the typically large areas covered by WT classifications, these studies revealed promising results. However, the main limitation of the station–based reconstructions that are currently available is that they use relatively simple statistical approaches (i.e. the shortest Mahalanobis distance (SMD) from a defined centroid) that only capture the most prominent features of atmospheric circulation patterns and that they are restricted to using continuous data such as pressure and temperature. Especially during the early instrumental period, such quantitative data is scarce, whereas qualitative meteorological information from weather diaries is more widely available. More complex approaches that can detect patterns in more detail and make use of qualitative data could improve existing WT reconstructions and might even allow for extending them backwards in time, where even less quantitative information is available.

Whereas common statistical approaches have been effective in capturing prominent atmospheric patterns, their ability to handle more complex, non-linear relationships and incorporate qualitative data is limited. Supervised machine learning (ML) classification methods offer a promising alternative, as they are well suited for recognizing intricate non-linear patterns in atmospheric variables. Furthermore, they can handle mixed data types, i.e. they could also include qualitative data on past weather in a categorised form. Nowadays, machine learning is commonly used for classification and pattern recognition in meteorological and climatological research, ranging from detection of extreme events (Racah et al., 2017; Chattopadhyay et al., 2020), frontal systems (Dagon et al., 2022; Bochenek et al., 2021; Biard and Kunkel, 2019), blocking situations (Muszynski et al., 2021; Thomas et al., 2021) or storms and cyclone tracks (Accarino et al., 2023; Kumler-Bonfanti et al., 2020; Mittermeier et al.,

2019; Williams et al., 2008). In the specific context of WT reconstruction, however, ML is still a rather novel approach. Schlef et al. (2019) used neural networks to detect circulation patterns associated with extreme floods in the US. Luferov and Fedotova (2020) used a convolutional neural network to reconstruct Dzerdzeevskii WTs for the northern hemisphere (Dzerdzeevskii, 1962). Mittermeier et al. (2022) studied WT pattern changes in the context of climate change using ML classifications of the Grosswetterlagen (general WTs) for central Europe after Hess and Brezowsky (1952). Whereas the abovementioned pioneering work of WT reconstruction is entirely based on gridded data from atmospheric reanalyses, an application of ML approaches to station–based WT classification in order to reconstruct long–term WT series is currently lacking.

In our study, we address this gap by assessing different machine learning approaches for station–based WT reconstruction over Europe. Our aim is to demonstrate the potential of different ML approaches for this task, but also their limitations. For this method intercomparison, we use the CAP9 WT classification representative of central Europe (Weusthoff, 2011). As CAP9 is an objective (i.e. based on statistical approaches) WT classification based on a cluster analysis of principal components from reanalysis pressure data, it does not suffer from the aforementioned issues with subjective WT classes and thus provides an ideal testbed for training and evaluating our ML approaches. Our study pursues two aims: i) providing an encompassing assessment of different ML approaches for the purpose of objective WT classification using station observations and ii) extending the CAP9 WT reconstruction to the period 1728–2022. Our assessment of the ML approaches is performed with the same input data that Schwander et al. (2017) used for their Mahalanobis distance–based approach, which serves as a baseline for comparison. The reconstruction methods are compared using a simplification of the CAP9 WT classification with seven WTs (CAP7) introduced for the baseline approach due to methodological limitations (see Schwander et al., 2017). We assess logistic regression, random forests, as well as classical, recurrent and convolutional neural network approaches. The most powerful model from this comparison is then retained to reconstruct daily CAP9 WTs back to 1728 from an extended set of station data. For this reconstruction, additional station series that became available in recent years were included (see Sect. 2.2). The reliability of the WT reconstructions is evaluated in detail to provide a robust basis for eventual applications of this WT series, as well as to explore possible room for improvement for future attempts in WT classification. In view of the ability of ML approaches to use also categorical information, we provide a short assessment of the impact of including time series of wet days as model input. A more encompassing analysis of the effect of using qualitative data for WT reconstruction – especially data on wind direction which would provide valuable information on atmospheric circulation – must be left for future research as currently long–term, homogeneous time series are virtually inexistent.

The article is organised as follows: Sect. 2 gives an overview of the data and machine learning approaches used for WT reconstruction, as well as the model tuning strategy. Results and discussion are presented in Sect. 3. The first part shows a detailed intercomparison of the station–based WT reconstruction methods on the example of CAP7 WTs. The second part analyses the extended CAP9 reconstruction using the best model from the comparison. Summary and conclusions are given in Sect. 4.

2 Data & Methods

2.1 Weather types

From the abundant number of WT classifications for Europe (see Philipp et al., 2010, 2016, for an overview), we use the CAP9 WT classification as produced and continuously updated by MeteoSwiss (Weusthoff, 2011). The CAP9 classification was chosen as it is objective (see discussion in Sect. 1) and because it has been shown to be a reliable predictor of surface climatic conditions in the Alpine region (Schiemann and Frei, 2010). Furthermore, a manageable amount of nine WTs – e.g. compared to the 29 WTs after Hess and Brezowsky (1952) – was found to be more suitable for assessing our ML approaches. Given the scarcity of meteorological records in the early instrumental period, classifications with abundant WTs could not be accurately represented by the few observation sites.

This WT classification is based on the CAP (Cluster Analysis of Principal Components) method (for details see Weusthoff, 2011; Philipp et al., 2010; Comrie, 1996; Ekström et al., 2002): in the first step, the gridded atmospheric variables are rearranged into a time x gridcell matrix and then decomposed into their principal components to which a Varimax rotation is applied for better interpretability of the loadings (see Ekström et al., 2002). The principal component scores are then clustered in the second step (non-hierarchical clustering with predefined class number that minimizes within-class dispersion) to derive WT classes. The CAP9 classification by MeteoSwiss was derived from mean sea level pressure from the ERA40 reanalysis (Kållberg et al., 2004; Uppala et al., 2005), whereas the attribution to the nine WTs in operational use is based on the Euclidean distance from the respective pressure centroids of the ERA40–derived WTs (Weusthoff, 2011).

The daily time series of CAP9 WTs from 01.09.1957–31.12.2020 used as predictand for the model training and as reference series for the analyses in Sect. 3 was obtained from MeteoSwiss. An overview of the synoptic situation of the different WTs is given in Fig. 1 (left). Shown are filled contours of average sea level pressure derived from the ERA5 reanalysis (Hersbach et al., 2020; Bell et al., 2021) over the period 1957–2020. Whereas there are seven types associated with advective patterns for the Alpine region, only WTs 5 and 8 are dominated by convective circulation (Fig. 1, top right; categorization in convective and advective WTs after Weusthoff, 2011). Note that the CAP9 WTs have different persistence lengths and different occurrence frequencies with some WTs showing strong seasonal patterns (Fig. 1, bottom right). For our model comparison (Sect. 3.1), we use a reduced set of seven WTs (CAP7) in order to compare the results directly with the Mahalanobis distance approach in Schwander et al. (2017). They found types 5 and 8, as well as 7 and 9 in the CAP9 classification hard to distinguish and merged the respective WT pairs. While we merge the same pairs for the analyses in Sect. 3.1, the machine learning models are trained on the original CAP9 WTs.

For our reconstruction, the WT classification has to be assumed stationary over time, meaning that the dominant circulation patterns over central Europe remained the same for the last 300 years. Our WT reconstruction thus does not yield information on whether the characteristics of the prevailing synoptic situations changed, which due to the scarcity of data for the earlier periods covered by our reconstruction is not possible. This stationarity assumption is further discussed in Sect. 3.

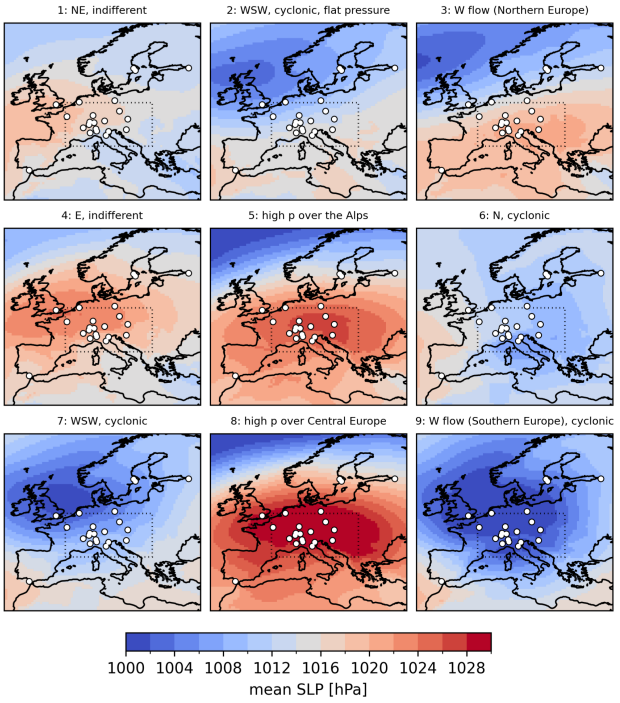

Type	Description	circulation	persistence
1	NorthEast, indifferent	advective	7.00 days
2	West-SouthWest, cyclonic, flat pressure	advective	4.89 days
3	Westerly flow over Northern Europe	advective	4.92 days
4	East, indifferent	advective	5.23 days
5	High Pressure over the Alps	convective	6.02 days
6	North, cyclonic	advective	4.59 days
7	West-SouthWest, cyclonic	advective	3.94 days
8	High Pressure over Central Europe	convective	6.25 days
9	Westerly flow over Southern Europe, Cyclonic	advective	3.53 days

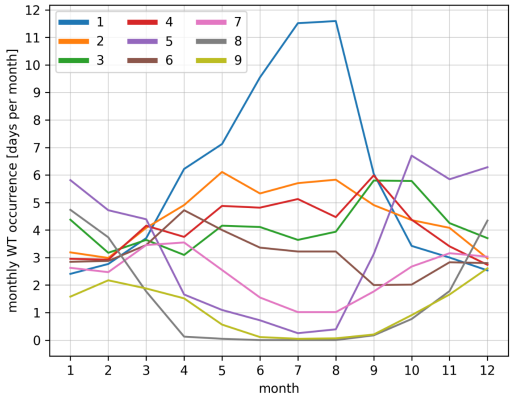

Figure 1. Left: climatological average of sea level pressure 1957–2020 for CAP9 WTs. White filled circles indicate station locations (see Sect. 2.2). The dotted rectangle represents the wider Alpine area for which the CAP9 WT classification is representative. Right: description of CAP9 WTs including their average persitence [days] in the period 1957–2020 (top) and their average monthly occurrence 1957–2020 (bottom).

2.2 Station observations

Meteorological observations used for WT reconstruction are located around and within the greater Alpine region in central Europe, for which the CAP9 classification is representative (Fig. 1; see also Weusthoff, 2011). Note that the available stations are relatively well distributed across central Europe, which is crucial to capture the large–scale synoptic situation. However, in southern and eastern Europe available digitised station records unfortunately were scarce. Whereas the CAP9 classification is based solely on sea level pressure data, the station observations used for our reconstructions also include other variables, i.e. temperature and categorical rain data. Sea level pressure represents the synoptic atmospheric flow, whereas the other variables represent the associated surface effects and thus may provide valuable additional information for WT reconstruction (Schwander et al., 2017), especially in the context of the early instrumental period with scarce data availability. A summary of the available daily station records is given in Table 1 with the data source indicated in the last column.

Table 1: daily meteorological data used for WT reconstructions. t = temperature, p = pressure, Δp = temporal pressure gradient, rr = wet days

ID	Name	Lat	Lon	Alt (m a.s.l.)	Variables	Period	Source / Comments
BAS	Basel	47.541	7.584	316	t,	1756–2020	CHIMES (Brönnimann and Brugnara, 2020, 2021),
					p, Δp	1764–2020	MeteoSwiss (Füllemann et al., 2011; Begert et al.,
					rr	1864–2020	2005)
BER	Bern	46.991	7.464	552	t,	1781–2020	CHIMES (Brugnara et al., 2022a), MeteoSwiss
					p, Δp	1781–2020	(Füllemann et al., 2011; Begert et al., 2005)
BRL	Berlin	52.456	13.300	40	p, Δp	1728–2020	DWD (Behrendt et al., 2011; Kaspar et al., 2013);
					rr	1876–2020	gap in pressure series 1771–1875
BOL	Bologna	44.497	11.353	53	t	1728–2020	Camuffo et al. (2017), ECA&D (Klein Tank et al.,
					rr	1818–2020	2002)
CAD	Cadiz	36.500	–6.260	1	t	1790–2020	IMPROVE (Camuffo and Jones, 2002; Barriendos
					p, Δp	1818–2020	et al., 2002), ECA&D (Klein Tank et al., 2002)
DBL	DeBilt	52.100	5.180	1	t	1738–2020	ECA&D (Klein Tank et al., 2002), Brandsma et al.
					p, Δp	1738–2020	(2000)
ENG	Engelberg	46.822	8.411	1035	rr	1864–2020	MeteoSwiss (Füllemann et al., 2011; Begert et al.,
							2005)
GVA	Geneva	46.248	6.128	410	t	1771–2020	CHIMES/DigiHom (Häderli et al., 2020;
					p, Δp	1818–2020	Brönnimann et al., 2020), MeteoSwiss (Füllemann
					rr	1864–2020	et al., 2011; Begert et al., 2005)
HPE	Hohenpeissenberg	47.800	11.020	995	t	1781–2020	Winkler (2006, 2009), DWD (Behrendt et al., 2011;
					p, Δp	1781–2020	Kaspar et al., 2013)
					rr	1818–2020	
KAR	Karlsruhe	49.039	8.365	112	t	1764–2020	Brugnara et al. (2015), DWD (Behrendt et al., 2011;
							Kaspar et al., 2013), ECA&D (Klein Tank et al.,
							2002); gaps 1790–1818, 1864–1876
LOH	Lohn	47.752	8.678	585	rr	1864–2020	MeteoSwiss (Füllemann et al., 2011; Begert et al.,
							2005)
LDN	London	51.515	–0.120	1035	p, Δp	1728–2020	Cornes et al. (2012a), ECA&D (Klein Tank et al.,
							2002)
LUG	Lugano	46.000	8.970	273	t	1864–2020	MeteoSwiss (Füllemann et al., 2011; Begert et al.,
					p, Δp	1864–2020	2005)
					rr	1864–2020	
MIL	Milan	45.470	9.180	132	t	1764–2020	IMPROVE (Moberg et al., 2000; Maugeri et al.,
					p, Δp	1874–2020	2002), ECA&D (Klein Tank et al., 2002)
OXF	Oxford	51.760	–1.260	63	rr	1864–2020	ECA&D (Klein Tank et al., 2002)
PAD	Padua	45.398	11.800	12	t	1781–2020	IMPROVE (Camuffo and Jones, 2002; Camuffo
					p, Δp	1728–2020	et al., 2006), Brugnara et al. (2015), ECA&D
							(Klein Tank et al., 2002)
PAR	Paris	48.817	2.322	77	t	1876–2020	Cornes et al. (2012b), ECA&D (Klein Tank et al.,
					p, Δp	1749–2020	2002)

PRA	Prague	50.090	14.420	190	t	1781–2020	Kyselý (2007), Stepanek (2005), ECA&D (Klein Tank et al., 2002)
SAM	Samedan	46.526	9.879	1708	rr	1864–2020	MeteoSwiss (Füllemann et al., 2011; Begert et al., 2005)
STK	Stockholm	59.350	18.050	44	t	1756–2020	IMPROVE (Moberg et al., 2000), ECA&D (Klein Tank et al., 2002)
					p, Δp	1756–2020	
					rr	1864–2020	
SPE	St. Petersburg	59.967	30.300	3	t	1756–2020	IMPROVE (Camuffo and Jones, 2002), ECA&D (Klein Tank et al., 2002)
TOR	Turin	45.070	7.680	281	t	1756–2020	Di Napoli and Mercalli (2008), ECA&D (Klein Tank et al., 2002)
					p, Δp	1818–2020	
UPP	Uppsala	59.861	17.641	15	t	1728–2020	IMPROVE (Moberg et al., 2000; Bergström and Moberg, 2002), ECA&D (Klein Tank et al., 2002)
					p, Δp	1728–2020	
WIE	Vienna	48.249	16.356	198	t	1781–2020	GeoSphere Austria (2021); gap in temperature series 1818–1864
					p, Δp	1864–2020	
					rr	1864–2020	
ZAG	Zagreb	45.820	15.980	156	t	1864–2020	ECA&D (Klein Tank et al., 2002)
					p, Δp	1864–2020	
SMA	Zurich	47.378	8.566	555	t	1764–2020	CHIMES (Brugnara et al., 2022a), MeteoSwiss (Füllemann et al., 2011; Begert et al., 2005); gap in pressure series 1790–1818
					p, Δp	1764–2020	
					rr	1864–2020	

For the comparison of reconstruction methods (Sect. 3.1), we use the same set of stations and variables that were used by Schwander et al. (2017) without any further preprocessing (see the SMD station sets in Fig. 2). This encompasses station records from London (Cornes et al., 2012a), Milan, Uppsala, Stockholm (Moberg et al., 2000; Maugeri et al., 2002), Turin (Di Napoli and Mercalli, 2008), Prague (Kyselý, 2007; Stepanek, 2005; Brázdil et al., 2012), Hohenpeissenberg (Winkler, 2009), De Bilt (Klein Tank et al., 2002), Paris (Cornes et al., 2012b, only temperature), Bern, and Lugano (Füllemann et al., 2011; Begert et al., 2005). Using the same data allows for a direct comparison between our machine learning approaches and the Mahalanobis distance–based method used in Schwander et al. (2017). In accordance with the latter study, daily mean temperature, sea level pressure and the computed pressure difference to the previous day (Δp, cf. Table 1) were used as input variables for this comparison.

Further early instrumental station series have been made available as a result of data rescue efforts in recent years (Brönnimann et al., 2019; Brugnara et al., 2020b), enhancing the data coverage in our area of interest and extending the period for which WTs can be reconstructed. Unfortunately, the majority of available records covers only a few years and thus is not suitable for our purpose. Using short observation records would lead to varying sets of stations, which on the one hand would introduce inconsistencies in reconstructed WTs and on the other hand constitute immense computational efforts, as for each set of stations a new model has to be trained. Further issues arise from inhomogeneities in the observation series in time (e.g. observation errors, artificial trends or shifts), which originate from changes in instruments or observation sites, as well as var-

ious error sources related to early instrumental data (see e.g. Brugnara et al., 2020a; Winkler, 2006; Böhm et al., 2010). Such inhomogeneities would again lead to errors or biases in the reconstructed WT series.

Where possible, long–term, homogenised station records that contain no or only few and short gaps were used for our approach. For some locations, however, multiple historical observation records from the same location had to be merged into a single time series. For the temperature series from Bern, Basel, Geneva and Zurich, we could benefit from previous efforts to merge and homogenise daily temperature series (Brugnara et al., 2022a). Only stations at close locations, i.e. within a radius of less than 15 km, have been merged, with the exceptions of Cadiz (merged with T and p data from Huelva) and De Bilt (merged with T data from Haarlem and p data from Zwanenburg, Haarlem, Den Helder and Delft), where the existing series could not be complemented with nearby station records. Complementary series have been retrieved from the ECA&D database (Klein Tank et al., 2002), as well as from the databases of MeteoSwiss (Füllemann et al., 2011; Begert et al., 2005), the German weather service DWD (Behrendt et al., 2011; Kaspar et al., 2013), the Royal Netherlands Meteorological Institute KNMI (Brandsma et al., 2000), and (GeoSphere Austria, 2021, formerly Austrian Central Institution for Meteorology and Geodynamics ZAMG). The station sets used for the method comparison and the reconstruction of CAP9 WTs (Sects. 3.1 and 3.3) are summarised in Fig. 2 labeled according to their respective start date. Whereas the comparisons in Sect. 3.1 use temporal pressure gradients as input, these gradients were omitted for the CAP9 reconstructions (Sect. 3.2 and 3.3) as tests (not shown) did not reveal consistent improvements by adding this variable.

Whereas in Schwander et al. (2017) observation records had not been homogenised, we deemed it suitable to apply such a procedure to all pressure and temperature series that had not been homogenised, as well as to the merged series. We used the break point detection approach by Wang and Feng (2018) combining a penalised maximal t test (Wang et al., 2007) and a penalised maximal F test (Wang, 2008). As reference series, we used monthly pressure and temperature series extracted for the respective station locations from the EKF400v2 reanalysis (Valler et al., 2022). For further details on this homogenisation approach, see Imfeld et al. (2023). Most of the homogenised station records exhibit no or smaller gaps with a median of 31 days. All gaps up to a length of 5 years were imputed with a k nearest neighbor approach following Batista and Monard (2002). This is the same approach also used by Schwander et al. (2017) for their WT reconstructions, thus keeping the consistency in our datasets. Tests for the imputation approach with 25 % randomly introduced gaps revealed an average bias of –0.063 hPa (–0.05 °C) and a mean absolute error of 1.83 hPa (1.46 °C) for pressure (and temperature). We thus deemed this method suitable for the task of WT reconstruction. The series from Berlin, Karlsruhe, Vienna (temperature) and Zurich (pressure) have longer gaps in their station record, which were kept.

Further preprocessing was necessary to use the station observations in the different machine learning models (the results of the respective assessments are not shown). First of all, a global warming trend is visible in all temperature records. In order to establish robust classification models, such non–stationarities in the data had to be removed. Temperature trends were removed individually for each series using a 3rd order polynomial fit. Furthermore, the pronounced seasonality of temperature might blur temperature signals originating from atmospheric dynamics and lead to an inhomogeneous treatment of weather types throughout the year. Thus, temperature data were corrected for seasonality by fitting the first two harmonics to each temperature record and then subtracting these harmonics from the data. Pressure and precipitation data have not been corrected

a) pressure

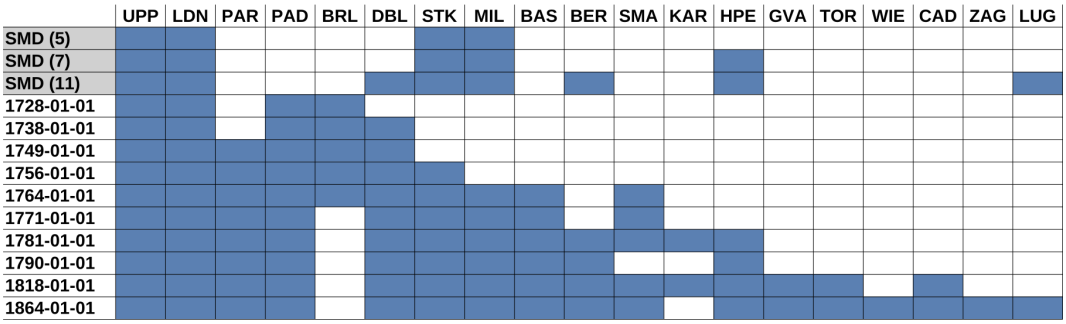

b) temperature

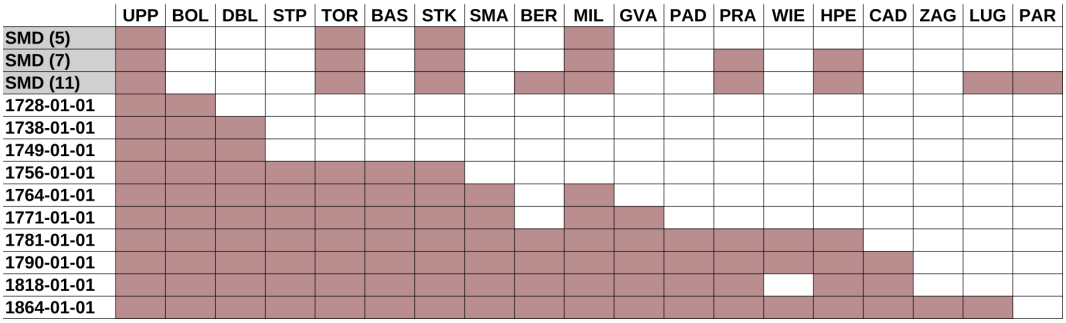

Figure 2. Station sets of a) sea level pressure and b) temperature used for the model comparison and WT reconstruction. The top three rows (SMD, grey shaded) refer to the station sets in Schwander et al. (2017) with 5, 7 and 11 stations, respectively. Station sets indicated with a date are used for the CAP9 reconstruction. The date refers to the start date of the respective station set. Data availability is indicated by the filled blue (pressure) and red (temperature) squares.

for a trend or seasonality, which contribute only a negligible part to the total variability of these variables. All variables from all stations were standardised (i.e. by subtracting their average and dividing by their standard deviation). An important point to mention is that pressure gradients and thus atmospheric patterns are less pronounced in summer than in winter (see e.g. Fig. 5 in Sect. 3.3). Although the general spatial distribution of the pattern remains similar throughout the year, the same WT shows different pressure amplitudes depending on the season. This might lead to seasonal inconsistencies in the WT reconstructions (see discussion in Sect. 3.1 and 3.3). To correct for this issue, a monthly standardisation of pressure was tested (not shown). However, this deteriorated the reconstructions and was thus dismissed.

2.3 Machine Learning Approaches

For our model comparison (Sect. 3.1) multiple machine learning models are tested and compared against a baseline WT classification approach. This baseline model is given by the simple statistical classification approach by Schwander et al. (2017) for their CAP7 reconstructions and is based on the shortest Mahalanobis distance (SMD) of station observations to the centroids

(station data averages) for each WT previously calculated from the reference period data. Further details on this approach are expounded in Schwander et al. (2017). The focus of this section lies on the ML approaches, including a multinomial logistic regression model, a random forest model, feed forward neural networks, as well as recurrent and convolutional neural networks. The best performing model is then selected for the reconstruction of daily CAP9 WTs back to 1728 (see Sect. 3.3).

2.3.1 Multinomial Logistic Regression (MLG)

Multiple logistic regression is a commonly used method for classification problems with categorical outcome. With a multiple logistic regression model, we can predict the occurrence probability p of a weather class WT as a function of several different station observations $x_1, x_2, ..., x_n$ as independent variables (Hosmer and Lemeshow, 2000). Whereas multiple logistic regression can predict only a binary dependent variable y, multnomial logistic regression can handle several response classes (given that they have no natural order). The occurrence probability $p(x)$ is defined as:

$$y = p(x) = \frac{1}{1 + e^{(-g(x))}}, \text{ where } 0 \leq p(x) \leq 1$$

The model is based on a linear regression function $g(x)$:

$$g(x) = \beta_0 + \beta_1 x_1 + \beta_2 x_2 + ... + \beta_n x_n$$

The regression coefficients β_n are computed applying the maximum likelihood method to maximise the probability, meaning that the coefficients are determined iteratively. For details see the documentation of R's caret package (Kuhn, 2008).

Compared to complex and more advanced machine learning methods, logistic regression has the advantage of interpretability, as the relationships between predictors and predictand can be directly inferred. One major drawback, however, is that often only a small number of covariates can be used in a model, as an increasing number of covariates may be subject to multicollinearity, which consequently can lead to overfitting of the model. To avoid this, we limited the number of predictors to five and constrained the variance inflation factor (VIF) to values below four. Model overfitting is further restrained by the training procedure (see Sect 2.4). Furthermore, one has to keep in mind that logistic regression only allows for a linear combination of covariates, thus non–linear features in the predictor data with respect to WTs are not captured by MLG.

2.3.2 Random Forests (RF)

The second machine learning approach assessed in this paper are random forests (RF) (Ho, 1995; Breiman, 2001). In contrast to single decision trees, RF use an ensemble of decision trees built from subsamples of the training data. With an increasing number of trees, the generalisation error of RF models decreases and robust predictions can be established. In the case of our classification application, RF can provide a probabilistic estimate of the true WT using their ensemble of decision trees. Compared to other machine learning approaches, RF are fast to train (depending on the number of trees), but can suffer from overfitting. In order to find a RF architecture with an optimal balance between accuracy and generalisability, several parameter sets are tested. These encompass the number of trees (between 10 and 400), the maximum depth (between 5 and 30), the

minimum sample size for splitting (between 2 and 10) and the minimum sample size for a leaf (between 1 and 4). Furthermore, the Gini impurity and entropy were tested for determining the splits. For further information see the documentation of the scikit–learn python package (Pedregosa et al., 2011).

2.3.3 Feedforward Neural Networks (NN)

The second approach are feedforward neural networks (NN) (Rosenblatt, 1958; Hastie et al., 2009). Similar to the RF approach, NN provide estimates of probability for each class, represented by the normalised weights of the output layer. The NN architecture used for our work is not based on a pre–designed NN model. While we prescribed the use of multiple layers, including a dropout layer before the output layer to avoid overfitting, optimal architectural properties such as the number of layers and their sizes were determined from scratch with a hyperparameter search on the training data (see also Sect. 2.4). In particular, networks with a number of layers between 2 and 8 were tested with layer sizes between 32 and 256 (in steps of 32). Furthermore, dropout rates between 0.05 and 0.2 (in steps of 0.05), as well as learning rates between 10^{-4} and 10^{-2} were tested during model tuning. The models were trained using the Adam optimisation algorithm (Kingma and Ba, 2014) and the categorical crossentropy loss function. We set the batch size to 200 and the maximum number of epochs to 50 (with early stopping with a patience of five epochs). The NN approach, as well as the other neural network approaches were implemented using Tensorflow (Abadi et al., 2016a, b) and Keras (Chollet, 2021) libraries.

2.3.4 Recurrent and Convolutional Neural Networks (RNN & CNN)

Both, the RF and the NN models described above use input data from the same day as predictors. As circulation patterns can persist for several days, it might be beneficial to also include information from preceeding days in our models. For this reason, we assess both recurrent neural networks (RNN) and 1D–convolutional neural networks (CNN) in this study. For the RNN we used so–called long–short–term memory networks (LSTM) that can retain or discard information from previous time steps, thus being able to propagate relevant information over multiple time steps (Hochreiter and Schmidhuber, 1997). Our RNN architecture follows the one of the NN, again with a dropout layer before the output layer and the same settings for model training. For reasons of computational costs, less architectural configurations were assessed than for the NN (i.e. between 2 and 5 layers with sizes between 32 and 128).

Similar to RNNs, convolutional neural networks (CNN) can also make use of data from previous timesteps. Whereas CNN is mostly applied to image data or other multi–dimensional datasets for pattern detection using trained filters (Fukushima, 1980), we used its 1–dimensional equivalent for time series analysis (Kiranyaz et al., 2021). Like for the RNN, a reduced set of architectural properties (i.e. between 2 and 5 layers with sizes between 32 and 128) has been assessed, while the rest of the tunable parameters were kept identical to the other networks.

For both time–dependent neural networks (RNN and CNN), we used data from two days prior to the day of interest (three days in total) to predict the WTs. A longer time window was found not to yield improvements in the results (not shown). Analogous to NN, RNN and CNN were also trained using the Adam optimisation algorithm with the categorical crossentropy loss function, a batch size of 200 and a maximum of 50 epochs with early stopping.

2.4 Hyperparameter Tuning and Validation

Training and validation of the machine learning approaches was performed with the data described in Sect. 2.1 and 2.2 using the station observations as predictors and the CAP9 WT classification as predictand. For the model comparison (Sect. 3.1), temperature, pressure, and temporal pressure gradients were used as predictors as in the baseline approach (Schwander et al., 2017). The CAP9 reconstructions (Sects. 3.2 and 3.3) only use pressure and temperature series, as tests revealed no consistent improvements from including pressure gradients (not shown). After preliminary tests with certain subsets of stations and atmospheric variables (not shown), which did not yield any clear gain in performance, we chose to use the full set of stations and variables (pressure and temperature) available for the respective periods. For their approach, Schwander et al. (2017) used a reduced set of seven WTs (CAP7). Two pairs of WTs, 5 (high pressure over the Alps) and 8 (high pressure over central Europe), as well as 7 (west–southwest, cyclonic) and 9 (westerly flow over southern Europe, cyclonic) were combined to single WTs, as they were found to be too similar to distinguish. In order to compare our machine learning models to the SMD approach in Schwander et al. (2017) in our model comparison (Sect. 3.1), the former are trained on the same station data as used in the original study, but with the CAP9 WTs as predictand. To make validation measures comparable to the baseline model, CAP9 classes are subsequently converted to CAP7 by combining the pairs of WTs accordingly. Also the reference period for the model comparison (Sect. 3.1) was chosen similar to the baseline study by Schwander et al. (2017), spanning 01.01.1961–31.12.1998. For our new WT reconstructions (Sect. 3.3), we made use of the full available period for model training spanning 01.09.1957–31.12.2020 and used the CAP9 classification for the evaluation.

Note that the same data is used for both hyperparameter tuning and validation of the models. In order to ensure independence between model tuning and evaluation, a nested cross–validation (Cawley and Talbot, 2010) is implemented. For the RF and neural network approaches, an outer loop splits the data into a training and an independent test set. An inner loop is applied to the training set for hyperparameter tuning, again splitting off part of the data for validation of the model configurations in order to find the optimal hyperparameters independent from the training data. The outer loop then serves to independently estimate the validation metrics. Optimal hyperparameters are determined using Bayesian optimisation (Snoek et al., 2012). A total number of 8 folds for the outer loop and 7 folds for the inner loop without shuffling and without overlap are applied. For the MLG model, we followed the same structure of outer and inner loops, but with 10 outer and 10 inner folds (with overlap) instead of 8 and 7. The outer loop splits the data randomly into 80 % training and 20 % independent testing datasets. The inner loop uses the 80 % folds for finding the best combination of station variables, again splitting into 70 % of the data for training and 30 % for validation. We find the best combination and best number of predictors manually with a bidirectional stepwise approach, looking at mean performance, significance and z values of predictors. Once a model was found that worked well on all 10 inner folds and showed a good balance between over– and underfitting, we retrained it with the 80 % sets and evaluated with the independent test sets (20 %) in the outer loop.

As Schwander et al. (2017) did not perform an independent validation of their approach, validation measures are not comparable. For this reason, we reconstructed their approach and applied a cross–validation with the same training and test splits as in the eight outer loops described above. Results from this independent cross–validation can be directly compared to our approaches. When reconstructing the Mahalanobis distance approach of Schwander et al. (2017), an error in their model setup became apparent: when calculating the distance to each WT centroid using the covariance matrix *derived for the respective* WT, considerably lower accuracies than indicated in the original study were obtained (not shown). However, using the covariance matrix from the *true (observed)* WT, which of course would be unknown for the reconstructions, accuracies reached the values from the original study. For our validation of the SMD approach, the distance was calculated for each WT centroid using the correct covariance matrix of the respective WT.

Model performance is estimated with the overall accuracy and average Heidke skill score (HSS; Heidke, 1926; Cohen, 1960) values for all WTs and all seasons. The overall accuracy represents the fraction or percentage of days for which the WTs were correctly classified. The HSS represents the proportion of correct predictions scaled by the expected correct forecasts due to chance for categorical forecasts (see Hyvärinen, 2014) and is calculated for each WT. In contrast to overall accuracy, the HSS accounts for differences in the occurrence of individual WTs. To obtain a robust and independent estimate of the true performance of the best models, an average of these validation measures is taken over the outer folds of the nested cross–validation (i.e. ten and eight test sets for MLG and the other approaches, respectively). Note that the model used for the WT time series reconstruction is retrained with the full available dataset within the validation period. Indicated accuracies for the individual models are thus arguably pessimistic.

3 Results & Discussion

3.1 Model Intercomparison for CAP7 weather types

The performance of the WT classification approaches presented in Sect. 2.3, as well as the SMD approach by Schwander et al. (2017) for the CAP7 WT classification is indicated in Table 2. Shown accuracies and HSS represent an average from the k–fold cross–validation over the period 01.01.1961–31.12.1998 (see Sect. 2.4) based on three different subsets with data from five, seven and eleven stations, respectively, as used in (Schwander et al., 2017, see also Table 3 therein). For the logistic regression model, only results from the optimal selection of station series is shown (see Sect. 2.3). The best–performing MLG model uses the following six variables: pressure in Milan and Paris, temperature in Prague and Stockholm, and the temporal pressure gradient in Milan and Stockholm.

Table 2: Validation metrics of all applied approaches for CAP7 WT reconstruction, as well as the baseline model (SMD, grey shaded) using different data subsets. The value before the slash indicates average accuracy in percent, the value after the slash indicates the Heidke Skill Score. Shown are values for the whole year (ANN), and the individual seasons (winter: DJF, spring: MAM, summer: JJA, autumn: SON). Highest values per station set are marked in bold

Station Set	**Model**	**ANN**	**DJF**	**MAM**	**JJA**	**SON**
custom selection of variables & stations	MLG	74.5 / 0.70	74.3 / 0.71	74.4 / 0.70	73.8 / 0.67	75.3 / 0.71
SMD (5 stations)	SMD	64.7 / 0.58	73.3 / 0.60	62.9 / 0.56	56.3 / 0.45	66.3 / 0.58
	RF	74.3 / 0.70	78.4 / 0.70	71.8 / 0.67	72.2 / 0.63	75.1 / 0.69
	NN	76.1 / 0.72	79.9 / **0.72**	73.7 / 0.70	73.7 / **0.65**	77.1 / 0.72
	RNN	**76.8 / 0.73**	**80.6 / 0.72**	**75.1 / 0.71**	**73.8 / 0.65**	**77.9 / 0.73**
	CNN	76.0 / 0.72	79.2 / 0.71	74.8 / **0.71**	72.4 / 0.63	77.7 / 0.72
SMD (7 stations)	SMD	67.4 / 0.61	75.7 / 0.64	66.3 / 0.61	59.0 / 0.48	68.8 / 0.61
	RF	78.4 / 0.75	80.9 / 0.73	77.6 / 0.74	75.8 / 0.67	79.2 / 0.74
	NN	**81.6 / 0.78**	**84.5 / 0.78**	**81.1 / 0.78**	78.3 / 0.71	**82.4 / 0.78**
	RNN	80.5 / 0.77	83.1 / 0.76	79.5 / 0.76	78.1 / 0.71	81.3 / 0.77
	CNN	81.3 / **0.78**	83.3 / 0.76	80.4 / 0.77	**79.4 / 0.72**	81.9 / **0.78**
SMD (11 stations)	SMD	62.9 / 0.56	70.6 / 0.56	61.1 / 0.55	55.1 / 0.44	64.8 / 0.56
	RF	82.6 / 0.79	83.6 / 0.77	82.0 / 0.79	81.2 / 0.73	83.7 / 0.80
	NN	**85.7 / 0.83**	87.8 / 0.82	**84.8 / 0.82**	83.8 / 0.78	**86.6 / 0.83**
	RNN	85.4 / **0.83**	**88.2 / 0.83**	84.6 / **0.82**	83.1 / 0.78	85.8 / 0.82
	CNN	85.5 / **0.83**	87.2 / 0.82	84.7 / **0.82**	**84.4 / 0.79**	85.8 / 0.82

Evidently, all ML approaches outperform the baseline model (SMD, grey shaded) for all sets of stations. With an independent validation and correcting the error in the SMD model (see Sect. 2.4), accuracies are by far lower than indicated in Schwander et al. (2017) dropping below 70 % overall and below 60 % in the summer months. The machine learning approaches show accuracies of about 75 % even for the smallest set of stations (and the selection of the MLG). Accuracies of the RF models are typically lower by 2–3 % compared to the neural networks regardless of the station set. Validation measures improve with the number of stations, reaching a maximum overall accuracy of 85.7 % for the NN model with 11 stations. Note that in contrast, the SMD approach shows lower accuracy values for the largest station set than for the other two, pointing to issues arising from data quality or the spatial distribution of the station network for this approach. Heidke Skill Scores (HSS) show a similar pattern with scores between 0.7 and 0.83 (compared to values between 0.56 to 0.61 for SMD). The superiority of the machine learning approaches might be explained by their ability to (in theory) better fit non-linear relationships and interactions in the data compared to common statistical approaches (see also Sect. 2.3).

From the seasonal validation measures we see a slight drop in accuracy (stronger for the HSS) for spring and summer, which was also found in Schwander et al. (2017), especially for summer. Weaker pressure gradients hamper a robust detection of WTs for these months. The difference between spring/summer and autumn/winter, however, is much smaller for the machine learning approaches compared to SMD. All of our models are thus better capable of coping with seasonal differences although

some seasonal patterns in the accuracy remain.

Random forests and multinomial logistic regression allow some inference about the stations and variables that prove to be the most crucial for WT classification. Regarding the spatial distribution of the stations, it is less a high density of stations within the area for which the CAP9 classification is representative (see Fig. 1), but rather an even distribution of stations around the borders of this area that lead to the most accurate predictions. This becomes evident for the optimal selection in the MLG approach with all predictors being highly significant in the model ($p \leq 0.05$). The MLG coefficients for each covariant and for each WT are listed in the supplement (Sect. S.2), together with further illustrations displaying the relationship of each predictor to the probability of each class response in the model. Also, RF results underpin that a spatially well distributed station network is crucial for a robust WT classification. This is not surprising, as for WT classification the models benefit not from the localised effects in the station observations but the information on an atmospheric state over a larger region. In this context, more stations located in southern, eastern, and also western Europe (compare Fig. 1) could improve the accuracy of the models. Looking at the feature importance (i.e. for each feature (predictor) the average reduction of the Gini impurity or entropy in the split classes over all trees) in RF, pressure data show the highest importance, followed by temperature (see Sect. S.3 in the supplement). The temporal pressure gradient on the other hand showed lower importance values by one order of magnitude compared to the other variables. These results are robust also to the MLG model, where pressure showed the highest importance, followed by temperature and pressure gradient. We want to note, however, that the MLG models still always preferred a combination of all three types of information instead of using just pressure data. This holds equally for the other approaches where preliminary tests using only pressure data vs. using all variables confirmed the use of our multivariate input data (not shown).

The model comparison revealed that on average the feedforward neural network (NN) exhibits the highest accuracy and HSS estimates, although only slightly better than for RNN and CNN. Note that for particular station sets or seasons, RNN and CNN show better metrics than the feedforward NN. An interesting result is that, opposite to our expectations, including the temporal evolution of the previous days (linked e.g. to preferential WT transitions) as input in RNN and CNN did not yield clear improvements. Whereas this temporal information may yield benefits when only a small number of input series is available (see RNN results in Table 2), measurements from a single day are generally sufficient for correctly detecting WTs. The NN can be considered as the best model for another reason: in contrast to RNN (and a bit less so for CNN), it is considerably faster to train, making it favourable also from the computational resources perspective. Regarding this aspect, it is important to mention that the simplest approaches we tested (MLG, RF) are much less costly in terms of computation hours than neural networks. Depending on the task and the related goal of accuracy, using these simpler methods is thus highly recommended. From this point on, we will only use the feedforward neural network model for further analyses and the final reconstruction.

3.2 The Effect of Categorical Weather Data

As stated in the introduction, ML approaches have the advantage that they can simultaneously process continuous and categorical information. In this section, we assess the effect of including time series of wet days based on rain information (see Sect. 2.2) as additional model input, as they have proven to be very valuable for statistical weather reconstructions (Imfeld et al., 2023). For this purpose we trained an NN model for two different station sets used for our new reconstruction (Sect. 3.3), once without and once with adding the categorical rain series. Model building and validation has again been performed as described in Sect. 2.4. We used the station set available from 1728 (fewest predictors: 4 pressure & 2 temperature series; see Fig. 2) and the one available from 1864 (most predictors: 17 pressure & 18 temperature series; see Fig. 2) to analyse the impact of adding categorical data for different numbers of predictors. Both station sets were complemented with 13 series of wet days (Sect. 2.2). Note that these categorical rain records do not go as far back as 1728, but mostly only back to 1864 (see Table 1). In order to better illustrate the effect of adding categorical data, we decided to use all available wet day series for both experiments.

For the 1728 station set without wet day series, the overall accuracy is estimated at 77.8 % (see also Table 3). By adding wet days, this increased by 0.5 % to 78.3 %. While for the autumn and winter months, the accuracy increased by 1 %, it declined by 0.5 % for the summer months. For the 1864 station set, adding wet days to the predictors decreased total accuracy by 0.8 % to 86.5 % (compared to 87.3 % without wet days). Also, all seasonal accuracies show a decrease between 0.4 % and 1.3 %. This shows that adding wet day series to the model input leads to negligible changes in accuracy which are mostly within the range of uncertainty of model training (i.e. smaller than the variance of accuracy and HSS in the outer folds of model training). With very few pressure and temperature records available (i.e. for the 1728 station set), wet days can provide supplementary information for WT classification. However, in our case improvements were limited to autumn and winter where precipitation is largely determined by large–scale circulation, whereas for summer, the results are slightly less accurate when including rain observations, which is arguably linked to precipitation being more frequently driven by local convection. If abundant pressure and temperature series are available (i.e. for the 1864 station set), using wet days as predictors yields no benefits. In this context, we decided to omit wet day series for our final CAP9 reconstructions in Sect. 3.3.

3.3 Reconstructing CAP9 weather types 1728–2020

3.3.1 Model Performance and Reconstruction Quality

With the feedforward Neural Network (NN) outperforming the other approaches (Sect. 3.1), we extended the current WT series for the CAP9 classification back to 1728. In order to provide an estimate for the model performance and by that of the reliability of our CAP9 reconstructions, a validation procedure as described in Sect. 2.4 was applied. The station series (sea level pressure and temperature records) that have been used as predictors are described in Sect. 2.2. A summary on the resulting model architectures can be found in the supplement (Sect. S.4). Table 3 gives an overview of the validation results in the form of overall accuracy and average HSS for predicted CAP9 WTs vs. the original predictand time series (1957–2020) by MeteoSwiss for all station sets. Results are again given for the whole period and distinguished by season. The achieved accuracy using the smallest station set (stations available from 01.01.1728 to 31.12.1737) is already remarkably high with a

value of 77.8 % despite the limited set of available stations. Adding more station series generally improves the accuracy and skill score values (with some remaining variability depending on model training runs). Note that validation metrics shown in Table 3 only provide values with respect to the reference period 1957-2020. The actual values for the past periods may be lower due to larger uncertainties and errors in the data, but unfortunately cannot be determined due to the lack of a historical reference WT series. Whereas reconstructions for most station sets show slightly less skill and lower accuracies for the summer months (JJA), differences to the overall average remain small with values of approximately 1 % for accuracy and 0.1 for the HSS. Those seasonal differences in model skill are arguably linked to the model being trained over the full year (see discussion in Sect. 3.3.2)

Table 3: validation results for the feedforward NN models with different station sets (named after their start year). The value before the slash indicates average accuracy in percent, the value after the slash indicates the Heidke Skill Score. Shown are estimates over the whole year (ANN), and the individual seasons (winter: DJF, spring: MAM, summer: JJA, autumn: SON)

Station Set	**ANN**	**DJF**	**MAM**	**JJA**	**SON**
1728	77.8 / 0.76	78.9 / 0.75	77.0 / 0.75	77.8 / 0.69	77.6 / 0.74
1738	78.9 / 0.77	80.0 / 0.77	78.2 / 0.77	79.5 / 0.72	77.8 / 0.75
1749	82.8 / 0.81	84.0 / 0.81	82.7 / 0.81	81.6 / 0.73	82.9 / 0.80
1756	83.2 / 0.82	84.3 / 0.82	82.8 / 0.82	82.8 / 0.78	82.9 / 0.80
1764	84.8 / 0.84	85.6 / 0.83	85.2 / 0.84	83.4 / 0.76	85.1 / 0.83
1771	83.9 / 0.83	83.8 / 0.81	83.9 / 0.83	83.6 / 0.75	84.4 / 0.83
1781	84.8 / 0.83	84.6 / 0.82	85.0 / 0.84	84.8 / 0.77	84.8 / 0.83
1790	84.7 / 0.84	84.8 / 0.82	84.8 / 0.84	84.3 / 0.77	84.9 / 0.83
1818	84.3 / 0.83	84.1 / 0.81	84.6 / 0.83	83.9 / 0.73	84.7 / 0.83
1864	87.3 / 0.86	87.6 / 0.85	87.8 / 0.87	86.9 / 0.82	87.0 / 0.85

To provide more insight into the patterns of correctly and wrongly classified WTs and the reasons why the model is not able to assign certain WTs correctly, further analyses have been performed. Fig. 3 shows the confusion matrices for the station sets 1728 and 1864 for the reference period 1957–2020. Whereas accuracies may vary between the models, training runs and station sets, the actual WTs that are wrongly assigned for each true class are similar. For the "extreme" WTs 8 and 9, most false predictions – as expected – identified WTs 5 and 7, which show the most similar patterns to the correct WTs 8 and 9, respectively (compare Fig. 1). Whereas Schwander et al. (2017) found these two WT pairs hard to distinguish and reduced the number of WTs accordingly, the NN model accuracies for WTs 8 and 9 are comparable to the other WTs. The NN model is thus capable of correctly distinguishing between these "extreme" (i.e. with respect to the intensity and extent of high/low pressure systems) WTs and their less extreme counterparts.

Figure 4 shows the patterns of pressure deviations from the average of the time series (in standard deviations) for each station and weather type within the reference period. Indicated are the average values for correctly assigned (blue) and wrongly assigned (red) WTs, as well as the range between the 5 % and 95 % quantiles (shaded areas) from the reconstruction with the 1864 station set. Deviations of the red and blue circles at individual/all observation points indicate regional/overall discrepan-

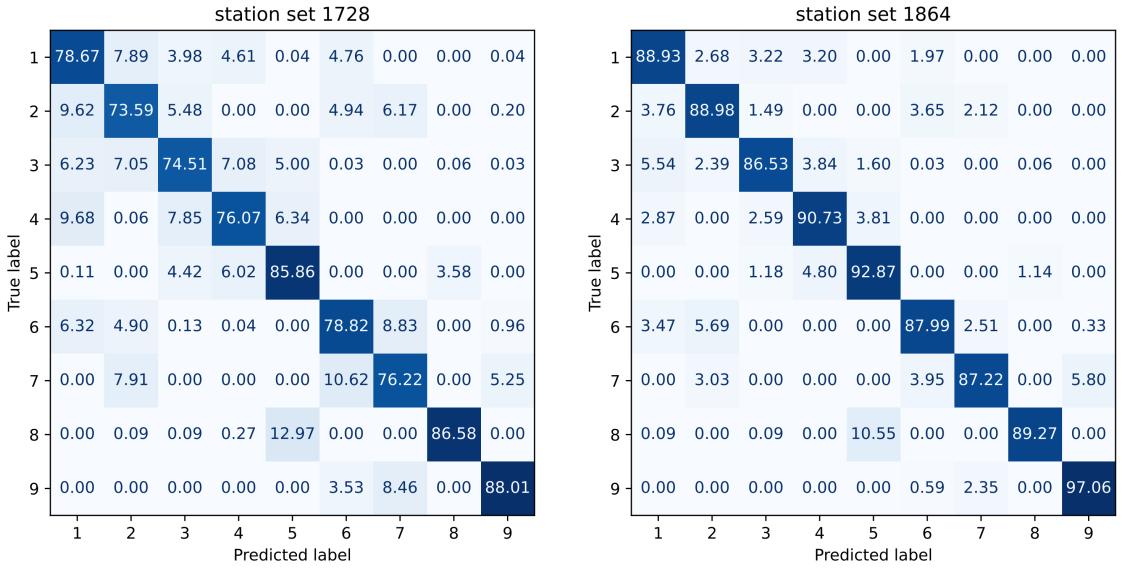

Figure 3. confusion matrices for reconstructions (columns) with station sets 1728 (left) and 1864 (right) against reference CAP9 series (rows) for the reference period. Values are given in percent of the respective WT occurrence.

cies in the observed pressure distribution as reason for false detection. Coinciding red and blue circles mean that observation patterns of true and false predictions are identical and that the reason for false predictions cannot be explained by the observations. Evidently, some WTs have very similar patterns with a large overlap (e.g. WT 5 and WT 8) making a distinction difficult. For most WTs dominated by extremely high or low pressure (e.g. WTs 5, 8, and 9), wrongly assigned WTs are linked to more moderate values in the pressure data. Furthermore, regional differences in the pressure distribution can be identified as a source of error. For example, WT 6 is more likely to be confused with other WTs for days with stronger low pressure systems over northern Central Europe. Such regional patterns can also be found for WTs 3, 4, and 7. The corresponding temperature profiles (see supplement Fig. S5.1) show similar patterns with observed temperatures for days with wrongly assigned WTs closer to the mean (WTs 2, 3, and 6) or regional differences (WTs 7, 8, and 9), although these patterns are much less distinct. The same evaluation for the other station sets provides similar results (not shown).

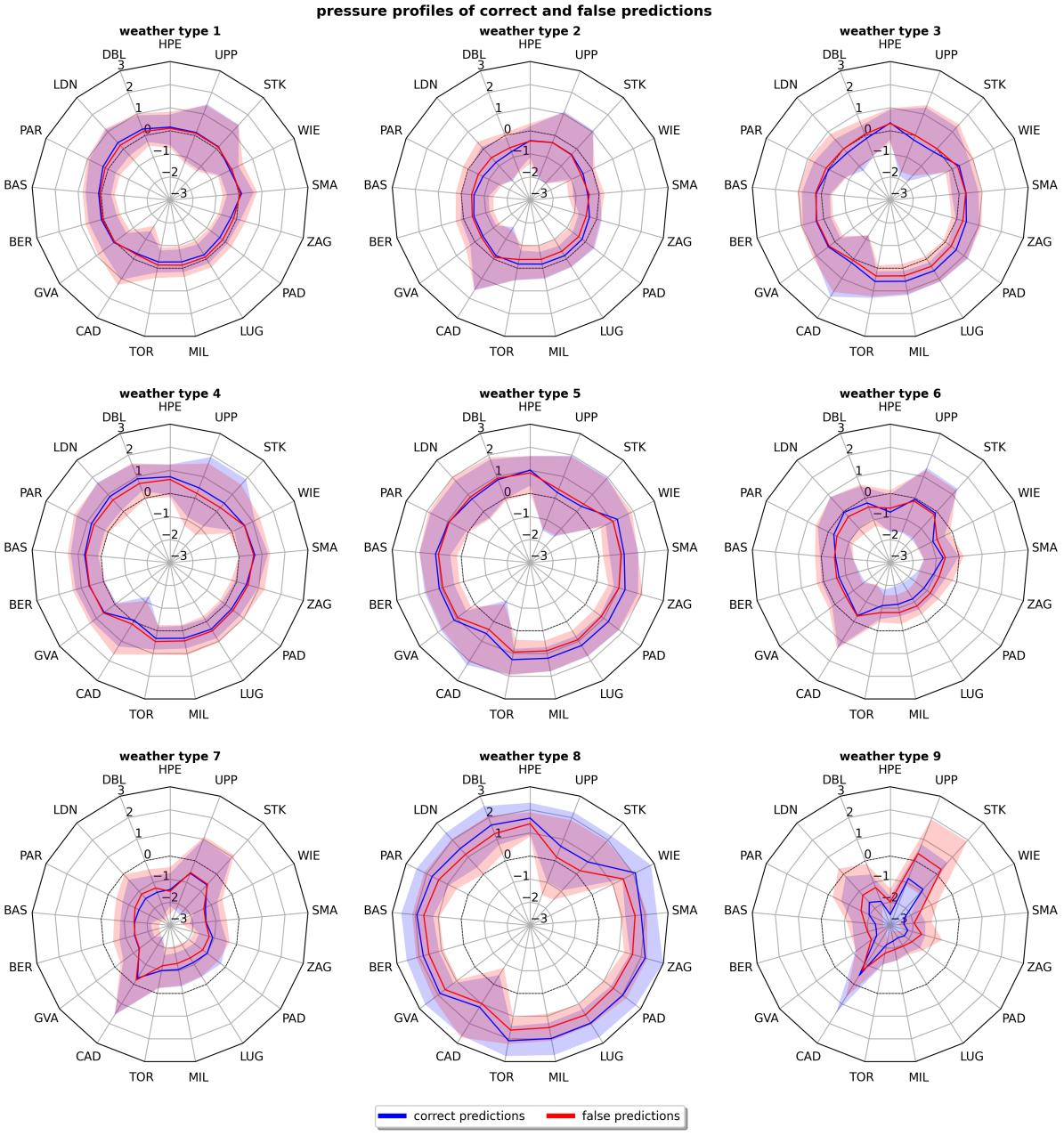

Figure 4. Station data pressure patterns for correct (blue) and false (red) predictions from the 1864 station set for all nine WTs. Shown are average (lines) and the 5 % – 95 % quantile interval (shaded areas) in units of standard deviations.

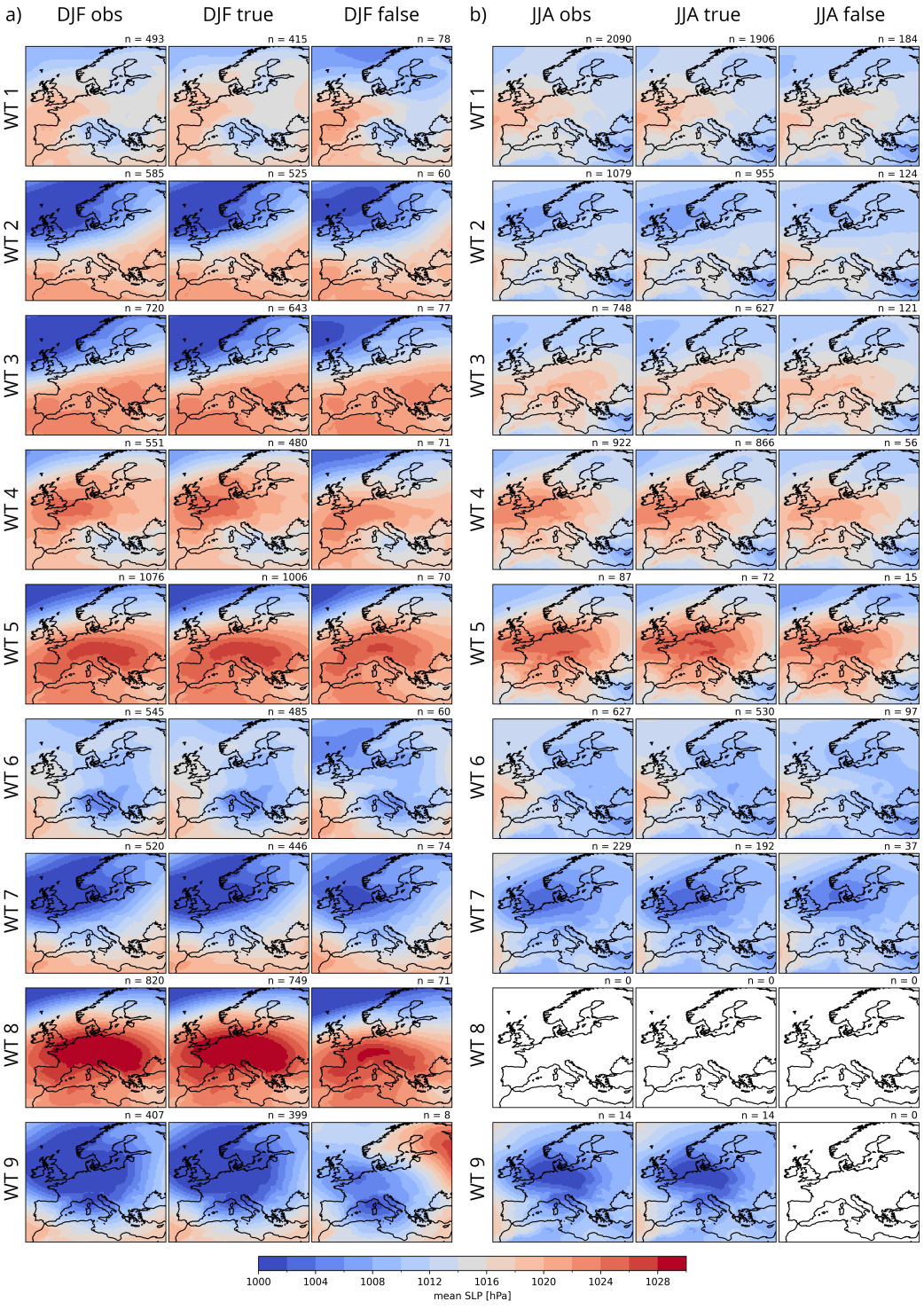

Figure 5. Climatological average of sea level pressure 1957–2020 for CAP9 WTs for a) the winter and b) the summer months. Shown are the averages according to the official WT series by MeteoSwiss (left, obs), correctly predicted WTs (centre, true) and wrongly predicted WTs (right, false). The number of cases (n) is indicated in the top right corner of each panel.

Figure 5 shows average sea level pressure maps for the period 1957–2020 derived from ERA5 (Hersbach et al., 2020; Bell et al., 2021). The maps are separated by season, namely winter (DJF, Fig. 5a) and summer (JJA, Fig. 5b), as well as by reference series (top), correctly attributed WTs (centre) and false predictions (bottom). Note that WT 8 does not occur during the summer months (see the seasonality in Fig. 1, as well as Fig. S5.2 in the supplement) and that no day was wrongly assigned to WT 9 in the reference period, hence the empty panels in Fig. 5b. Whereas false predictions for the winter months are strongly dominated by weaker–than–average pressure distribution rather than regional shifts, results are less clear for the summer months. Whereas slight regional shifts are apparent (e.g. for WTs 1, 3, and 7), the reason for false predictions in summer seems to originate from other sources, arguably patterns in temperature or general difficulties of the model to capture the smaller pressure gradients in this season.

Transitions between weather types may follow preferential patterns. A comparison of preferential transitions in the CAP9 reference series with reconstructions for the reference period from different station sets (Fig. S5.3 a-c in the supplement) did not show strong differences, although reconstructions show a small bias towards persistence. Our analyses furthermore revealed that those preferential transitions show only small changes throughout the reconstruction period (Fig. S5.3 d-f in the supplement). Preferential transitions between WTs are thus generally well represented in the CAP9 reconstructions. As the synoptic circulation is constantly changing, weather types might change over the course of one day. This has to be taken into account when analysing daily WT reconstructions, as such WT transitions may be a source of error. In the reference CAP9 series, 19.1 % of days are persistent weather situations with the same WT on the days before and after. A majority of days (46.4 %) is a partly transient situation with the same WT on one of the neighboring days and a different one on the other and in 34.5 % of the cases, different WTs occur on both neighboring days (transient situation). Taking reconstructions using station set 1864 as an example, the correctly classified WTs show the same percentages. For the days with false predictions, however, transient situations are overrepresented (48.0 %), whereas only 7.6 % show persistent conditions. We can conclude that transient situations play an important role as a source of uncertainty in daily WT reconstructions. The chosen WT for these cases typically is the one with the strongest imprint on the daily average station observations and not necessarily the one persisting throughout most of the day. Furthermore, a dominating WT might be chosen by a very small margin. This issue might be solved by introducing a neutral (transient) class or by calculating WTs for a specific time of the day (e.g. 12:00 UTC) using subdaily data which is, however, less readily available for the early instrumental period.

A next interesting feature to look at is the confidence of the model in its predictions, i.e. the probabilities with which the WTs are classified. As stated in Sect. 2.3, for each day the NN attributes a probability to all WT classes and the respective class with the highest probability is selected as the predicted (or most likely) WT. Figure 6a (for comparison with the baseline approach see Fig. S5.4 in the supplement) shows a one–year running mean of the daily probabilities of the predicted WTs by season for the whole period of reconstruction. It shows values around 0.8 in the first two decades, increasing to values between 0.825 and 0.875 in the middle of the 18th century and to values between 0.85 and 0.9 in 1864. The fact that detection probabilities remain nearly constant at a high level over the last 300 years suggests that the stationarity assumption of the WT classification (see Sect. 2.1) is reasonable, as otherwise larger shifts towards lower detection probabilities would be expected.

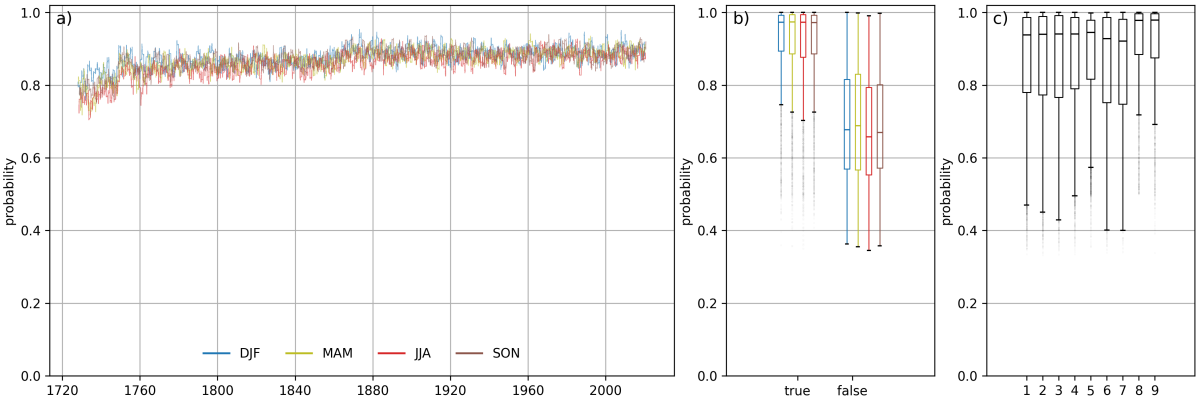

Figure 6. a) 1-year running mean of the daily maximum probability (fraction) of the reconstructed CAP9 WT series separated by season. b) boxplots of the probability for correctly (true) and wrongly (false) attributed WTs within the reference period separated by season. c) as in b) but separated by weather type. The thick line indicates the median, the boxes extend to the quartiles and whiskers to 1.5 times the interquartile range

Also the seasonal differences in detection probabilities are small. The distinction of daily maximum probabilities by correct and false classifications in the reference period (Fig. 6b) reveals that the model used for our CAP9 reconstruction is less confident for WTs that were wrongly assigned (median = 67.4 %) than for correct attributions (median = 97.3 %). This is in line with the above finding on transient WTs that mixed signals in the surface observations may lead to false classifications. Seasonal differences are again small with only slightly lower values in summer, showing that the model being trained over the full year can be considered reasonable. The same applies to differences in detection probability between individual WTs (Fig 6c). Only the two "extreme" WTs 8 and 9 show slightly different patterns (i.e. higher probabilities).

3.3.2 The new CAP9 Reconstructions in a Climatological Context

In this section, we look at the CAP9 WT reconstructions produced with the chosen NN approach (Sect. 2.3) for the full period 1728–2022. The aim is to analyse their quality and consistency, i.e. look for possible discontinuities in WT frequencies, as they have e.g. been found for the Hess & Brezowski WT classification in the mid–1980s (Mittermeier et al., 2022). Furthermore, we compare occurrence frequencies of reconstructed CAP9 WTs with the CAP9 reference series on climatological timescales to analyse the representation of internal climate variability of WTs in the past decades to centuries. For a comparison with the WT reconstruction by Schwander et al. (2017), the supplement provides figures as presented in this section including the CAP7 reconstructions (see Fig. S5.4–S5.6).

An important quality characteristic are biases in the occurrence of different WTs. Figure 7 illustrates the percentual bias (with respect to the number of days of the year) in yearly WT occurrence for the reference period (n = 63 years) separated by station set and weather type (for comparison with the baseline approach see Fig. S5.5 in the supplement). The median biases

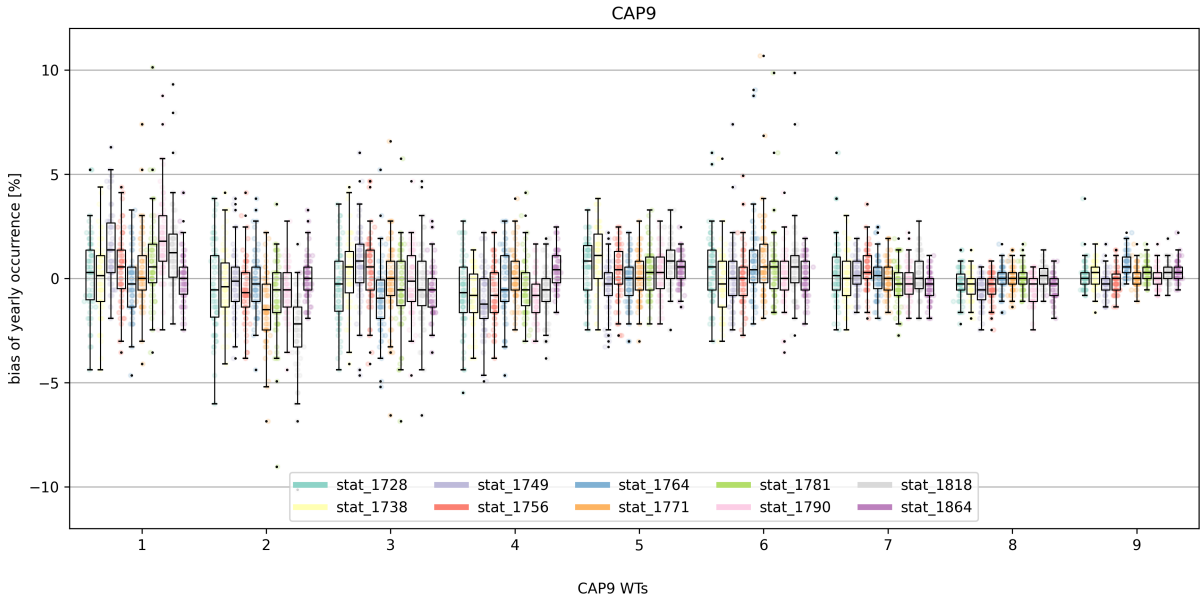

Figure 7. Bias of yearly WT occurrence (in % of days of the year) for all WTs (x–axis) and station sets (colors) in the NN reconstruction.

remain within 1–2 % for all WTs and station sets with no systematic over– or underestimation of an individual WT. Some outlier years are evident for WTs 1, 3 and 6 (overestimation), as well as WTs 2 and 3 (underestimation).

Figure 8 illustrates the full reconstructed time series of the yearly occurrence for each WT (in black), again with the CAP9 reference series (in red) for comparison (A comparison with the baseline approach is given in Fig. S5.6 in the supplement). For better readability, a 10–year running average is indicated. The yearly WT occurrence in our new CAP9 reconstruction shows high correlation values (average = 0.948) and relatively low root mean squared error values (average = 3.35 days). A positive bias for WTs 6 and 9, as well as a negative bias for WT 8 determined in Fig. 7 can also be seen in the time series. In the time series presented in Fig. 8, no apparent artificial discontinuities that go beyond natural variability can be determined, which is expected as homogenised input data is used. In order to study discontinuities and trends in further detail, statistical tests were applied. To detect discontinuities (i.e. changes in the data structure) in yearly WT occurrence, we applied a pruned exact linear time (PELT) algorithm as implemented in (Truong et al., 2020, see also Killick et al. (2012)) with the constraint that change points are 10 samples apart at least. Between 9 and 17 change points were detected over the full reconstruction period (Fig. S5.7 in the supplement). This analysis does not allow to infer if the detected discontinuities are artificial or originate from natural variability. However, only a few common breakpoints between individual WTs are found and the majority of detected discontinuities does not coincide with changed station sets in the input. This points to the fact that the discovered discontinuities are not introduced artificially and that our CAP9 reconstructions can be considered homogeneous over time. Long-term trends were examined using a Mann-Kendall test (Kendall, 1975) at a significance level of $\alpha = 0.05$. No significant trends in yearly occurrence have been found (see Fig. S5.8 in the supplement). These analyses support the stationarity assumption (see Sect.

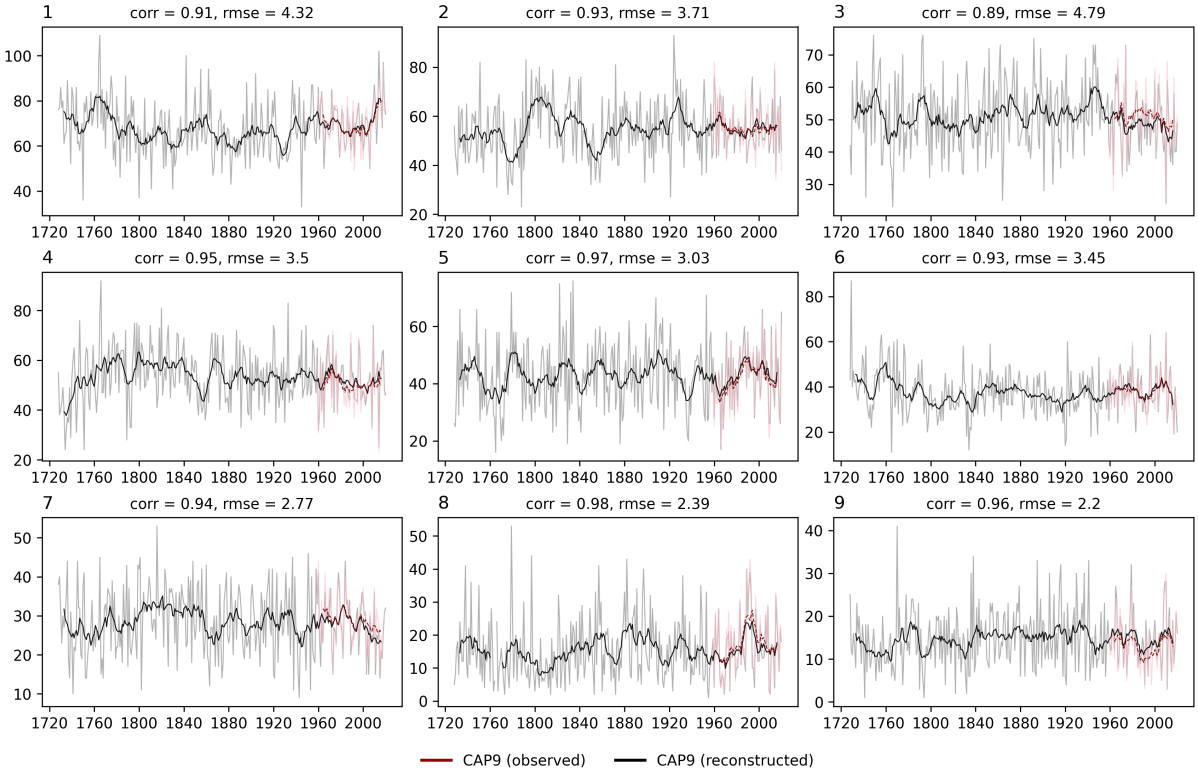

Figure 8. Yearly occurrence of reconstructed CAP9 WTs (lighter colors) with 10–year running mean (darker colors). Shown are the CAP9 reference series (red) and the CAP9 reconstructions (black). Indicated are correlation and root mean squared error for the yearly WT occurrence with respect to the reference series.

2.1). If this assumption were not to pertain, a pronounced decline in the frequency of occurrence would be expected, as the predefined modern WTs could only rarely be observed in the far past. For the yearly average persistence, however, statistically significant trends could be determined for WTs 4 (decrease), 7 (decrease), and 9 (increase), although small in magnitude (see Fig. S5.9 in the supplement).

More detail on the occurrence frequency is given in Fig. 9, where we show the 10–year running average yearly WT occurrence distinguished by season. These seasonal occurrence patterns of CAP9 reconstructions generally match the occurrence in the reference series. For WTs 6 and 9, the observed positive bias in the reconstructions can be mainly attributed to an overestimation of WT occurrence in spring (MAM). The negative bias of WT 8 on the other hand is linked to an underestimation of this WT in the winter months (DJF). The attribution of a bias to seasonal differences points to an important issue in WT reconstruction. As most WTs (1, 5, 7, 8, and 9) show a pronounced seasonality they can be difficult to predict for a model that is trained over all seasons. Tests with training individual models for each season improved the results, although for some WTs (e.g. WT 8 in summer), the available sample for model training becomes too small. Another option might be to include

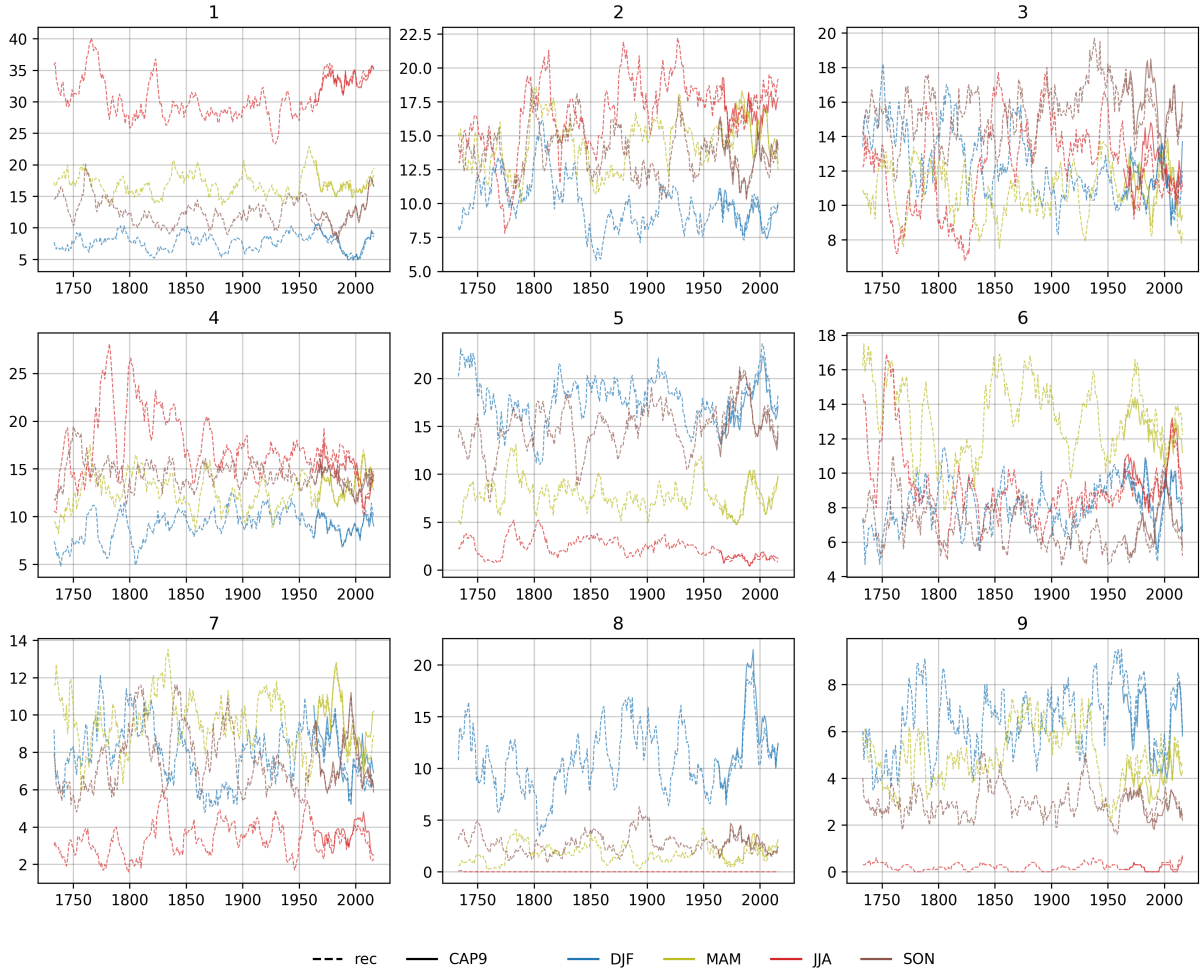

Figure 9. 10–year running average of yearly WT occurrence by season and WT. Shown are the CAP9 reference series (solid lines) and the CAP9 reconstructions (dashed lines).

seasons or months as categorical predictor variables, although this has not been tested in this study. Seasonal shifts of WT occurrence are assessed in Fig. S5.10 in the supplement. WT 1 exhibits a stronger seasonality in recent decades, whereas the seasonal variation of WTs 4 and 7 tend to decrease. The winter occurrence peak of WT 3 is shifted towards autumn and WT 2 shows a tendency towards a second occurrence peak in summer. However, those seasonal shifts are small compared to the large year-to-year variability of WTs.

4 Conclusions

In our study, we applied various supervised machine learning (ML) methods for station–based weather type (WT) reconstruction in order to assess their performance and to find an optimal ML approach for this purpose. With the model showing the best performance and using additional station observations, existing CAP9 WT series have been extended back to 1728.

Our results show that all ML approaches perform well when tested on the daily CAP7 WT classification. Independent estimates of accuracy and HSS show a better performance of all tested models compared to the common statistical classification approach used as a baseline. ML methods can indeed profit from their ability to detect non–linear patterns. The best performing method varies between the three tested neural network approaches depending on season, used data, and validation metric, although even the simpler and less computationally demanding multinomial linear regression and random forest approach yield good results. Overall, the feedforward neural network was found to be slightly better than the other ML approaches and was therefore used to create the CAP9 WT reconstruction. The use of qualitative rain observations did not improve our reconstructions, but instead yielded partially worse results and was thus omitted for our reconstructions. The extension of the existing CAP9 classification back to 1728 constitutes a novelty in WT reconstruction. The resulting WT time series proves to be accurate in various facets. No artificial trends or discontinuities could be detected. The year–to–year variability and the seasonality of the WTs are well reproduced. Nevertheless, depending on the available set of stations, some over– and underestimation of WT occurrence could be determined. Our results emphasise the importance of continuously improving methods of WT reconstruction with new options and data available.

Some challenges or limitations of our approach persist. First, the station data availability is usually scarce in the early instrumental period. Further data rescue efforts may provide additional observations at important locations for WT classifications. Although our experiment with adding qualitative rain information did not improve the reconstructions, other qualitative information more directly linked to large–scale circulation such as wind direction might lead to improvements. Unfortunately, the availability of digitised, long–term wind direction records is sparse and therefore could not be assessed in this study. A second challenge is the occurrence frequency of each WT in the reference series. WTs with low occurrence frequencies and strong seasonality can pose a challenge for our WT reconstruction approach. Adding seasons as additional predictors or training different models per season could solve this issue, although the sample size of rare WTs might be too small. Also in general, the size of the training dataset has to be proportionate to the number of WT classes in order to find robust model weights and biases. A third issue is the daily resolution of input and WT data: transient situations leave a mixed signal in the daily average observations making the distinction on a daily resolution difficult. This issue might be solved with the use of subdaily data which are, however, less readily available in the form of long and homogeneous time series.

Our CAP9 reconstruction represents the longest daily WT series available and allows for studying decadal circulation variability in the context of past climatic changes, as well as the impacts of associated synoptic situations on the surface, e.g.

extreme events. On the methodological side, future research may focus on including wind direction observations to improve and extend WT reconstructions even further back in time, although this requires tremendous digitisation efforts. Whereas we focused on reconstructing CAP9 WTs, our ML models may be adopted to other WT classifications and regions.

Code and data availability. Most station series used are publicly available on data repositories (Brugnara, 2022; ECA&D, 2024; GeoSphere Austria, 2021; DWD Climate Data Center, 2024). Observational records and weather types provided by MeteoSwiss can be directly obtained from MeteoSwiss on request. The reconstructed CAP9 WT series, as well as the corresponding code for model building and training is publicly available at the BORIS repository (Pfister, 2024, https://doi.org/10.48350/195666)

Author contributions. LP had the idea and planned the campaign with contributions from LW and SB. YB and NI provided observational data and code for homogenisation; LP and LW performed the computations, provided the visualisations, and wrote the manuscript. LW, SB, YB, and NI reviewed the manuscript.

Competing interests. The authors declare that they have no conflict of interest.

Acknowledgements. The authors would like to thank all the institutions that provided the valuable meteorological station observations (MeteoSwiss, DWD, GeoSphere Austria, KNMI). Particular thanks goes to Mikhaël Schwander for providing the original input data he used for his CAP7 reconstruction, as well as to Luis Rivero who performed insightful preliminary research testing neural networks for weather type reconstruction.

Funding. Lucas Pfister and Noemi Imfeld were funded by the Swiss National Foundation SNSF project "Daily Weather Reconstructions to Study Decadal Climate Swings". Additional funding for Yuri Brugnara and Lucas Pfister was available through the "Swiss Early Instrumental Meteorological Data" (CHIMES) project funded by SNSF and the "Long Swiss Meteorological Series" project funded by the Global Climate Observing System (GCOS) Switzerland. Lena Wilhelm was funded by the Swiss National Science Foundation (SNF) Grant CRSII5_201792.

References

Abadi, M., Agarwal, A., Barham, P., Brevdo, E., Chen, Z., Citro, C., Corrado, G. S., Davis, A., Dean, J., Devin, M., Ghemawat, S., Goodfellow, I., Harp, A., Irving, G., Isard, M., Jia, Y., Jozefowicz, R., Kaiser, L., Kudlur, M., Levenberg, J., Mane, D., Monga, R., Moore, S., Murray, D., Olah, C., Schuster, M., Shlens, J., Steiner, B., Sutskever, I., Talwar, K., Tucker, P., Vanhoucke, V., Vasudevan, V., Viegas, F., Vinyals, O., Warden, P., Wattenberg, M., Wicke, M., Yu, Y., and Zheng, X.: TensorFlow: Large-Scale Machine Learning on Heterogeneous Distributed Systems, arXiv [preprint], https://doi.org/10.48550/ARXIV.1603.04467, 2016a.

Abadi, M., Barham, P., Chen, J., Chen, Z., Davis, A., Dean, J., Devin, M., Ghemawat, S., Irving, G., Isard, M., Kudlur, M., Levenberg, J., Monga, R., Moore, S., Murray, D. G., Steiner, B., Tucker, P., Vasudevan, V., Warden, P., Wicke, M., Yu, Y., and Zheng, X.: TensorFlow: A system for large-scale machine learning, arXiv [preprint], https://doi.org/10.48550/ARXIV.1605.08695, 2016b.

Accarino, G., Donno, D., Immorlano, F., Elia, D., and Aloisio, G.: An Ensemble Machine Learning Approach for Tropical Cyclone Localization and Tracking From ERA5 Reanalysis Data, Earth and Space Science, 10, 2023EA003 106, https://doi.org/10.1029/2023EA003106, 2023.

Barriendos, M., Martín-Vide, J., Peña, J. C., and Rodríguez, R.: Daily Meteorological Observations in Cádiz – San Fernando. Analysis of the Documentary Sources and the Instrumental Data Content (1786–1996), Climatic Change, 53, 151–170, https://doi.org/10.1023/A:1014991430122, 2002.

Batista, G. E. A. P. A. and Monard, M. C.: A Study of K-Nearest Neighbour as an Imputation Method, in: Soft computing systems: design, management, and applications, edited by Abraham, A., Köppen, M., and Ruiz-del Solar, J., no. 87 in Frontiers in artificial intelligence and applications, pp. 251–260, IOS Press [u.a.], Amsterdam, meeting Name: HIS, 2002.

Begert, M., Schlegel, T., and Kirchhofer, W.: Homogeneous temperature and precipitation series of Switzerland from 1864 to 2000, International Journal of Climatology, 25, 65–80, https://doi.org/10.1002/joc.1118, 2005.

Behrendt, J., Penda, E., Finkler, A., Heil, U., and Polte-Rudolf, C.: Beschreibung der Datenbasis des NKDZ [Description of the Data Base of Germany's National Climate Data Centre], Tech. rep., Deutscher Wetterdienst, Offenbach, Germany, 2011.

Bell, B., Hersbach, H., Simmons, A., Berrisford, P., Dahlgren, P., Horányi, A., Muñoz-Sabater, J., Nicolas, J., Radu, R., Schepers, D., Soci, C., Villaume, S., Bidlot, J., Haimberger, L., Woollen, J., Buontempo, C., and Thépaut, J.: The ERA5 global reanalysis: Preliminary extension to 1950, Quarterly Journal of the Royal Meteorological Society, 147, 4186–4227, https://doi.org/10.1002/qj.4174, 2021.

Bergström, H. and Moberg, A.: Daily Air Temperature and Pressure Series for Uppsala (1722–1998), Climatic Change, 53, 213–252, https://doi.org/10.1023/A:1014983229213, 2002.

Biard, J. C. and Kunkel, K. E.: Automated detection of weather fronts using a deep learning neural network, Advances in Statistical Climatology, Meteorology and Oceanography, 5, 147–160, https://doi.org/10.5194/ascmo-5-147-2019, 2019.

Bochenek, B., Ustrnul, Z., Wypych, A., and Kubacka, D.: Machine Learning-Based Front Detection in Central Europe, Atmosphere, 12, 1312, https://doi.org/10.3390/atmos12101312, 2021.

Brandsma, T., Koek, F., Wallbrink, H., and Können, G.: Het KNMI-programma HISKLIM (HIStorisch KLIMaat) [The KNMI programme HISKLIM (Historical Climate)], Koninklijk Nederlands Meteorologisch Instituut, De Bilt, Netherlands, 2000.

Breiman, L.: Random Forests, Machine Learning, 45, 5–32, https://doi.org/10.1023/A:1010933404324, 2001.

Brugnara, Y., Auchmann, R., Brönnimann, S., Allan, R. J., Auer, I., Barriendos, M., Bergström, H., Bhend, J., Brázdil, R., Compo, G. P., Cornes, R. C., Dominguez-Castro, F., Van Engelen, A. F. V., Filipiak, J., Holopainen, J., Jourdain, S., Kunz, M., Luterbacher, J., Maugeri, M., Mercalli, L., Moberg, A., Mock, C. J., Pichard, G., Řezníčková, L., Van Der Schrier, G., Slonosky, V., Ustrnul, Z., Valente, M. A.,

Wypych, A., and Yin, X.: A collection of sub-daily pressure and temperature observations for the early instrumental period with a focus on the "year without a summer" 1816, Climate of the Past, 11, 1027–1047, https://doi.org/10.5194/cp-11-1027-2015, 2015.

Brugnara, Y., Good, E., Squintu, A. A., Van Der Schrier, G., and Brönnimann, S.: The EUSTACE global land station daily air temperature dataset, Geoscience Data Journal, 6, 189–204, https://doi.org/10.1002/gdj3.81, 2019.

Brugnara, Y., Flückiger, J., and Brönnimann, S.: Instruments, Procedures, Processing, and Analyses, in: Swiss Early Instrumental Meteorological Series, no. G96 in Geographica Bernensia, pp. 17–32, Institute of Geography, University of Bern, Bern, Switzerland, https://doi.org/10.4480/GB2020.G96.02, 2020a.

Brugnara, Y., Pfister, L., Villiger, L., Rohr, C., Isotta, F. A., and Brönnimann, S.: Early instrumental meteorological observations in Switzerland: 1708–1873, Earth System Science Data, 12, 1179–1190, https://doi.org/10.5194/essd-12-1179-2020, 2020b.

Brugnara, Y., Hari, C., Pfister, L., Valler, V., and Brönnimann, S.: Pre-industrial temperature variability on the Swiss Plateau derived from the instrumental daily series of Bern and Zurich, Climate of the Past, 18, 2357–2379, https://doi.org/10.5194/cp-18-2357-2022, 2022a.

Brugnara, Y., Horn, M., and Salvador, I.: Two new early instrumental records of air pressure and temperature for the southern European Alps, preprint, ESSD – Atmosphere/Meteorology, https://doi.org/10.5194/essd-2022-290, 2022b.

Brunet, M. and Jones, P.: Data rescue initiatives: bringing historical climate data into the 21st century, Climate Research, 47, 29–40, https://doi.org/10.3354/cr00960, 2011.

Brázdil, R., Zahradníček, P., Pišoft, P., Štěpánek, P., Bělínová, M., and Dobrovolný, P.: Temperature and precipitation fluctuations in the Czech Republic during the period of instrumental measurements, Theoretical and Applied Climatology, 110, 17–34, https://doi.org/10.1007/s00704-012-0604-3, 2012.

Brönnimann, S. and Brugnara, Y.: D'Annone's Meteorological Series from Basel, 1755–1804, in: Swiss Early Instrumental Meteorological Series, no. G96 in Geographica Bernensia, pp. 119–126, Institute of Geography, University of Bern, Bern, Switzerland, https://doi.org/10.4480/GB2020.G96.11, 2020.

Brönnimann, S. and Brugnara, Y.: Meteorological Series from Basel, 1825 – 1863, in: Swiss Early Instrumental Meteorological Series, no. G96 in Geographica Bernensia, pp. 127–138, Institute of Geography, University of Bern, Bern, Switzerland, https://doi.org/10.4480/GB2020.G96.12, 2021.

Brönnimann, S., Allan, R., Ashcroft, L., Baer, S., Barriendos, M., Brázdil, R., Brugnara, Y., Brunet, M., Brunetti, M., Chimani, B., Cornes, R., Domínguez-Castro, F., Filipiak, J., Founda, D., Herrera, R. G., Gergis, J., Grab, S., Hannak, L., Huhtamaa, H., Jacobsen, K. S., Jones, P., Jourdain, S., Kiss, A., Lin, K. E., Lorrey, A., Lundstad, E., Luterbacher, J., Mauelshagen, F., Maugeri, M., Maughan, N., Moberg, A., Neukom, R., Nicholson, S., Noone, S., Nordli, , Ólafsdóttir, K. B., Pearce, P. R., Pfister, L., Pribyl, K., Przybylak, R., Pudmenzky, C., Rasol, D., Reichenbach, D., Řezníčková, L., Rodrigo, F. S., Rohr, C., Skrynyk, O., Slonosky, V., Thorne, P., Valente, M. A., Vaquero, J. M., Westcottt, N. E., Williamson, F., and Wyszyński, P.: Unlocking Pre-1850 Instrumental Meteorological Records: A Global Inventory, Bulletin of the American Meteorological Society, 100, ES389–ES413, https://doi.org/10.1175/BAMS-D-19-0040.1, 2019.

Brönnimann, S., Bühler, M., and Brugnara, Y.: The Series from Geneva, 1798–1863, in: Swiss Early Instrumental Meteorological Series, no. G96 in Geographica Bernensia, pp. 47–59, Institute of Geography, University of Bern, Bern, Switzerland, https://doi.org/10.4480/GB2020.G96.04, 2020.

Böhm, R., Jones, P. D., Hiebl, J., Frank, D., Brunetti, M., and Maugeri, M.: The early instrumental warm-bias: a solution for long central European temperature series 1760–2007, Climatic Change, 101, 41–67, https://doi.org/10.1007/s10584-009-9649-4, 2010.

Cahynová, M. and Huth, R.: Enhanced lifetime of atmospheric circulation types over Europe: fact or fiction?, Tellus A: Dynamic Meteorology and Oceanography, 61, 407–416, https://doi.org/10.1111/j.1600-0870.2009.00393.x, 2009.

Camuffo, D. and Jones, P., eds.: Improved Understanding of Past Climatic Variability from Early Daily European Instrumental Sources, Springer, Dordrecht, Netherlands, https://doi.org/10.1007/978-94-010-0371-1, 2002.

Camuffo, D., Cocheo, C., and Sturaro, G.: Corrections of Systematic Errors, Data Homogenisation and Climatic Analysis of the Padova Pressure Series (1725-1999), Climatic Change, 78, 493–514, https://doi.org/10.1007/s10584-006-9052-3, 2006.

Camuffo, D., Della Valle, A., Bertolin, C., and Santorelli, E.: Temperature observations in Bologna, Italy, from 1715 to 1815: a comparison with other contemporary series and an overview of three centuries of changing climate, Climatic Change, 142, 7–22, https://doi.org/10.1007/s10584-017-1931-2, 2017.

Casado, M., Pastor, M., and Doblas-Reyes, F.: Links between circulation types and precipitation over Spain, Physics and Chemistry of the Earth, 35, 437–447, https://doi.org/10.1016/j.pce.2009.12.007, 2010.

Cawley, G. C. and Talbot, N. L. C.: On Over-fitting in Model Selection and Subsequent Selection Bias in Performance Evaluation, Journal of Machine Learning Research, 11, 2079–2107, https://doi.org/10.5555/1756006.1859921, 2010.

Chattopadhyay, A., Nabizadeh, E., and Hassanzadeh, P.: Analog Forecasting of Extreme-Causing Weather Patterns Using Deep Learning, Journal of Advances in Modeling Earth Systems, 12, e2019MS001 958, https://doi.org/10.1029/2019MS001958, 2020.

Chollet, F.: Deep learning with Python, Manning Publications, Shelter Island, NY, USA, 2nd edn., 2021.

Cohen, J.: A Coefficient of Agreement for Nominal Scales, Educational and Psychological Measurement, 20, 37–46, https://doi.org/10.1177/001316446002000104, 1960.

Compo, G. P., Whitaker, J. S., Sardeshmukh, P. D., Matsui, N., Allan, R. J., Yin, X., Gleason, B. E., Vose, R. S., Rutledge, G., Bessemoulin, P., Brönnimann, S., Brunet, M., Crouthamel, R. I., Grant, A. N., Groisman, P. Y., Jones, P. D., Kruk, M. C., Kruger, A. C., Marshall, G. J., Maugeri, M., Mok, H. Y., Nordli, , Ross, T. F., Trigo, R. M., Wang, X. L., Woodruff, S. D., and Worley, S. J.: The Twentieth Century Reanalysis Project, Quarterly Journal of the Royal Meteorological Society, 137, 1–28, https://doi.org/10.1002/qj.776, 2011.

Comrie, A. C.: An All-Season Synoptic Climatology of Air Pollution in the U.S.-Mexico Border Region, The Professional Geographer, 48, 237–251, https://doi.org/10.1111/j.0033-0124.1996.00237.x, 1996.

Cornes, R. C., Jones, P. D., Briffa, K. R., and Osborn, T. J.: A daily series of mean sea-level pressure for London, 1692–2007, International Journal of Climatology, 32, 641–656, https://doi.org/10.1002/joc.2301, 2012a.

Cornes, R. C., Jones, P. D., Briffa, K. R., and Osborn, T. J.: A daily series of mean sea-level pressure for Paris, 1670–2007, International Journal of Climatology, 32, 1135–1150, https://doi.org/10.1002/joc.2349, 2012b.

Dagon, K., Truesdale, J., Biard, J. C., Kunkel, K. E., Meehl, G. A., and Molina, M. J.: Machine Learning-Based Detection of Weather Fronts and Associated Extreme Precipitation in Historical and Future Climates, Journal of Geophysical Research: Atmospheres, 127, e2022JD037 038, https://doi.org/10.1029/2022JD037038, 2022.

Delaygue, G., Brönnimann, S., Jones, P. D., Blanchet, J., and Schwander, M.: Reconstruction of Lamb weather type series back to the eighteenth century, Climate Dynamics, 52, 6131–6148, https://doi.org/10.1007/s00382-018-4506-7, 2019.

Di Napoli, G. and Mercalli, L.: Il clima di Torino [The Climate of Turin], vol. 7 of *Memorie dell'atmosfera*, SMS (Società meteorologica subalpina), Turin, Italy, 2008.

Drücke, J., Borsche, M., James, P., Kaspar, F., Pfeifroth, U., Ahrens, B., and Trentmann, J.: Climatological analysis of solar and wind energy in Germany using the Grosswetterlagen classification, Renewable Energy, 164, 1254–1266, https://doi.org/10.1016/j.renene.2020.10.102, 2021.

Dzerdzeevskii, B.: Fluctuations of climate and of general circulation of the atmosphere in extra-tropical latitudes of the Northern Hemisphere and some problems of dynamic climatology, Tellus A: Dynamic Meteorology and Oceanography, 14, 328–336, https://doi.org/10.3402/tellusa.v14i3.9559, 1962.

Ekström, M., Jönsson, P., and Bärring, L.: Synoptic pressure patterns associated with major wind erosion events in southern Sweden (1973-1991), Climate Research, 23, 51–66, https://doi.org/10.3354/cr023051, 2002.

Fleig, A. K., Tallaksen, L. M., Hisdal, H., Stahl, K., and Hannah, D. M.: Inter-comparison of weather and circulation type classifications for hydrological drought development, Physics and Chemistry of the Earth, 35, 507–515, https://doi.org/10.1016/j.pce.2009.11.005, 2010.

Fukushima, K.: Neocognitron: A self-organizing neural network model for a mechanism of pattern recognition unaffected by shift in position, Biological Cybernetics, 36, 193–202, https://doi.org/10.1007/BF00344251, 1980.

Füllemann, C., Begert, M., Croci-Maspoli, M., and Brönnimann, S.: Digitalisieren und Homogenisieren von historischen Klimadaten des Swiss NBCN – Resultate aus DigiHom [Digitizing and Homogenizing historical Calimate Data of the Swiss National Basic Climatological Network - Results of the DigiHom Project], Tech. Rep. 236, MeteoSwiss, Zurich, Switzerland, 2011.

GeoSphere Austria: Messstationen Tagesdaten [Measuring Stations, Daily Data] [data set], https://doi.org/10.60669/GS6W-JD70, 2021.

Hastie, T., Tibshirani, R., and Friedman, J. H.: The elements of statistical learning: data mining, inference, and prediction, Springer series in statistics, Springer, New York, NY, USA, 2nd edn., 2009.

Heidke, P.: Berechnung Des Erfolges Und Der Güte Der Windstärkevorhersagen Im Sturmwarnungsdienst [Calculation of the Success Rate and Quality of Wind Speed Forecasts in Storm Forecasting], Geografiska Annaler, 8, 301–349, https://doi.org/10.1080/20014422.1926.11881138, 1926.

Hersbach, H., Bell, B., Berrisford, P., Hirahara, S., Horányi, A., Muñoz-Sabater, J., Nicolas, J., Peubey, C., Radu, R., Schepers, D., Simmons, A., Soci, C., Abdalla, S., Abellan, X., Balsamo, G., Bechtold, P., Biavati, G., Bidlot, J., Bonavita, M., De Chiara, G., Dahlgren, P., Dee, D., Diamantakis, M., Dragani, R., Flemming, J., Forbes, R., Fuentes, M., Geer, A., Haimberger, L., Healy, S., Hogan, R. J., Hólm, E., Janisková, M., Keeley, S., Laloyaux, P., Lopez, P., Lupu, C., Radnoti, G., De Rosnay, P., Rozum, I., Vamborg, F., Villaume, S., and Thépaut, J.: The ERA5 global reanalysis, Quarterly Journal of the Royal Meteorological Society, 146, 1999–2049, https://doi.org/10.1002/qj.3803, 2020.

Hess, P. and Brezowsky, H.: Katalog der Grosswetterlagen Europas [Catalog of the General Weather Types in Europe], Tech. Rep. 33, Deutscher Wetterdienst in der US-Zone, Bad Kissingen, Germany, 1952.

Ho, T. K.: Random decision forests, in: Proceedings of 3rd International Conference on Document Analysis and Recognition, vol. 1, pp. 278–282, IEEE Comput. Soc. Press, Montreal, Que., Canada, https://doi.org/10.1109/ICDAR.1995.598994, 1995.

Hochreiter, S. and Schmidhuber, J.: Long Short-Term Memory, Neural Computation, 9, 1735–1780, https://doi.org/10.1162/neco.1997.9.8.1735, 1997.

Hosmer, D. W. and Lemeshow, S.: Applied Logistic Regression, Wiley, New York, NY, USA, 1st edn., https://doi.org/10.1002/0471722146, 2000.

Hoy, A., Hänsel, S., and Maugeri, M.: An endless summer: 2018 heat episodes in Europe in the context of secular temperature variability and change, International Journal of Climatology, 40, 6315–6336, https://doi.org/10.1002/joc.6582, 2020.

Huth, R., Beck, C., Philipp, A., Demuzere, M., Ustrnul, Z., Cahynová, M., Kyselý, J., and Tveito, O. E.: Classifications of Atmospheric Circulation Patterns: Recent Advances and Applications, Annals of the New York Academy of Sciences, 1146, 105–152, https://doi.org/10.1196/annals.1446.019, 2008.

Hyvärinen, O.: A Probabilistic Derivation of Heidke Skill Score, Weather and Forecasting, 29, 177–181, https://doi.org/10.1175/WAF-D-13-00103.1, 2014.

Häderli, S., Pfister, S., Villiger, L., Brugnara, Y., and Brönnimann, S.: Two Meteorological Series from Geneva, 1782–1791, in: Swiss Early Instrumental Meteorological Series, no. G96 in Geographica Bernensia, pp. 33–46, Institute of Geography, University of Bern, Bern, Switzerland, https://doi.org/10.4480/GB2020.G96.03, 2020.

Imfeld, N., Pfister, L., Brugnara, Y., and Brönnimann, S.: A 258-year-long data set of temperature and precipitation fields for Switzerland since 1763, Climate of the Past, 19, 703–729, https://doi.org/10.5194/cp-19-703-2023, 2023.

James, P. M.: An objective classification method for Hess and Brezowsky Grosswetterlagen over Europe, Theoretical and Applied Climatology, 88, 17–42, https://doi.org/10.1007/s00704-006-0239-3, 2007.

Jones, P. D. and Lister, D. H.: The influence of the circulation on surface temperature and precipitation patterns over Europe, Climate of the Past, 5, 259–267, https://doi.org/10.5194/cp-5-259-2009, 2009.

Jones, P. D., Osborn, T. J., Harpham, C., and Briffa, K. R.: The development of Lamb weather types: from subjective analysis of weather charts to objective approaches using reanalyses, Weather, 69, 128–132, https://doi.org/10.1002/wea.2255, 2014.

Kaspar, F., Müller-Westermeier, G., Penda, E., Mächel, H., Zimmermann, K., Kaiser-Weiss, A., and Deutschländer, T.: Monitoring of climate change in Germany – data, products and services of Germany's National Climate Data Centre, Advances in Science and Research, 10, 99–106, https://doi.org/10.5194/asr-10-99-2013, 2013.

Kendall, M. G.: Rank correlation methods, Griffin, London, 4. ed., 2. impr edn., 1975.

Killick, R., Fearnhead, P., and Eckley, I. A.: Optimal Detection of Changepoints With a Linear Computational Cost, Journal of the American Statistical Association, 107, 1590–1598, https://doi.org/10.1080/01621459.2012.737745, 2012.

Kingma, D. P. and Ba, J.: Adam: A Method for Stochastic Optimization, arXiv [preprint], https://doi.org/10.48550/ARXIV.1412.6980, 2014.

Kiranyaz, S., Avci, O., Abdeljaber, O., Ince, T., Gabbouj, M., and Inman, D. J.: 1D convolutional neural networks and applications: A survey, Mechanical Systems and Signal Processing, 151, 107 398, https://doi.org/10.1016/j.ymssp.2020.107398, 2021.

Klein Tank, A. M. G., Wijngaard, J. B., Können, G. P., Böhm, R., Demarée, G., Gocheva, A., Mileta, M., Pashiardis, S., Hejkrlik, L., Kern-Hansen, C., Heino, R., Bessemoulin, P., Müller-Westermeier, G., Tzanakou, M., Szalai, S., Pálsdóttir, T., Fitzgerald, D., Rubin, S., Capaldo, M., Maugeri, M., Leitass, A., Bukantis, A., Aberfeld, R., Van Engelen, A. F. V., Forland, E., Mietus, M., Coelho, F., Mares, C., Razuvaev, V., Nieplova, E., Cegnar, T., Antonio López, J., Dahlström, B., Moberg, A., Kirchhofer, W., Ceylan, A., Pachaliuk, O., Alexander, L. V., and Petrovic, P.: Daily dataset of 20th-century surface air temperature and precipitation series for the European Climate Assessment, International Journal of Climatology, 22, 1441–1453, https://doi.org/10.1002/joc.773, 2002.

Kostopoulou, E. and Jones, P. D.: Comprehensive analysis of the climate variability in the eastern Mediterranean. Part II: relationships between atmospheric circulation patterns and surface climatic elements, International Journal of Climatology, 27, 1351–1371, https://doi.org/10.1002/joc.1466, 2007.

Kuhn, M.: Building Predictive Models in R Using the caret Package, Journal of Statistical Software, 28, 1–26, https://doi.org/10.18637/jss.v028.i05, 2008.

Kumler-Bonfanti, C., Stewart, J., Hall, D., and Govett, M.: Tropical and Extratropical Cyclone Detection Using Deep Learning, Journal of Applied Meteorology and Climatology, 59, 1971–1985, https://doi.org/10.1175/JAMC-D-20-0117.1, 2020.

Kučerová, M., Beck, C., Philipp, A., and Huth, R.: Trends in frequency and persistence of atmospheric circulation types over Europe derived from a multitude of classifications, International Journal of Climatology, 37, 2502–2521, https://doi.org/10.1002/joc.4861, 2017.

Kyselý, J.: Implications of enhanced persistence of atmospheric circulation for the occurrence and severity of temperature extremes, International Journal of Climatology, 27, 689–695, https://doi.org/10.1002/joc.1478, 2007.

Kållberg, P. W., Simmons, A., Uppala, S. M., and Fuentes, M.: The ERA-40 Archive, Tech. Rep. 17, ECMWF, Reading, UK, 2004.

Küttel, M., Luterbacher, J., and Wanner, H.: Multidecadal changes in winter circulation-climate relationship in Europe: frequency variations, within-type modifications, and long-term trends, Climate Dynamics, 36, 957–972, https://doi.org/10.1007/s00382-009-0737-y, 2011.

Lamb, H. H.: British Isles weather types and a register of the daily sequence of circulation patterns 1861-1971, vol. 116 of *Geophysical Memoirs*, H.M. Stationery Office, London, UK, 1972.

Li, F., Lin, Y., Guo, J., Wang, Y., Mao, L., Cui, Y., and Bai, Y.: Novel models to estimate hourly diffuse radiation fraction for global radiation based on weather type classification, Renewable Energy, 157, 1222–1232, https://doi.org/10.1016/j.renene.2020.05.080, 2020.

Lorenzo, M. N., Taboada, J. J., and Gimeno, L.: Links between circulation weather types and teleconnection patterns and their influence on precipitation patterns in Galicia (NW Spain), International Journal of Climatology, 28, 1493–1505, https://doi.org/10.1002/joc.1646, 2008.

Luferov, V. and Fedotova, E.: A Deep Learning Approach to Recognition of the Atmospheric Circulation Regimes, in: Progress in Computer Recognition Systems, edited by Burduk, R., Kurzynski, M., and Wozniak, M., vol. 977, pp. 195–204, Springer, Cham, Switzerland, http://link.springer.com/10.1007/978-3-030-19738-4_20, 2020.

Maugeri, M., Buffoni, L., Delmonte, B., and Fassina, A.: Daily Milan Temperature and Pressure Series (1763–1998): Completing and Homogenising the Data, Climatic Change, 53, 119–149, https://doi.org/10.1023/A:1014923027396, 2002.

Minářová, J., Müller, M., Clappier, A., and Kašpar, M.: Characteristics of extreme precipitation in the Vosges Mountains region (north-eastern France), International Journal of Climatology, 37, 4529–4542, https://doi.org/10.1002/joc.5102, 2017.

Mittermeier, M., Braun, M., Hofstätter, M., Wang, Y., and Ludwig, R.: Detecting Climate Change Effects on Vb Cyclones in a 50-Member Single-Model Ensemble Using Machine Learning, Geophysical Research Letters, 46, 14 653–14 661, https://doi.org/10.1029/2019GL084969, 2019.

Mittermeier, M., Weigert, M., Rügamer, D., Küchenhoff, H., and Ludwig, R.: A deep learning based classification of atmospheric circulation types over Europe: projection of future changes in a CMIP6 large ensemble, Environmental Research Letters, 17, 084 021, https://doi.org/10.1088/1748-9326/ac8068, 2022.

Moberg, A., Jones, P. D., Barriendos, M., Bergström, H., Camuffo, D., Cocheo, C., Davies, T. D., Demarée, G., Martin-Vide, J., Maugeri, M., Rodriguez, R., and Verhoeve, T.: Day-to-day temperature variability trends in 160- to 275-year-long European instrumental records, Journal of Geophysical Research: Atmospheres, 105, 22 849–22 868, https://doi.org/10.1029/2000JD900300, 2000.

Muszynski, G., Prabhat, Balewski, J., Kashinath, K., Wehner, M., and Kurlin, V.: Atmospheric Blocking Pattern Recognition in Global Climate Model Simulation Data, in: 2020 25th International Conference on Pattern Recognition (ICPR), pp. 677–684, IEEE, Milan, Italy, https://doi.org/10.1109/ICPR48806.2021.9412736, 2021.

O'Hare, G. and Sweeney, J.: Lamb's Circulation Types and British Weather: An Evaluation, Geography, 78, 43–60, 1993.

Paegle, J. N.: Prediction of Precipitation Probability Based on 500-Mb Flow Types, Journal of Applied Meteorology, 13, 213–220, https://doi.org/10.1175/1520-0450(1974)013<0213:POPPBO>2.0.CO;2, 1974.

Pedregosa, F., Varoquaux, G., Gramfort, A., Michel, V., Thirion, B., Grisel, O., Blondel, M., Prettenhofer, P., Weiss, R., Dubourg, V., Vanderplas, J., Passos, A., Cournapeau, D., Brucher, M., Perrot, M., and Duchesnay, : Scikit-learn: Machine Learning in Python, Journal of Machine Learning Research, 12, 2825–2830, http://jmlr.org/papers/v12/pedregosa11a.html, 2011.

Petrow, T., Zimmer, J., and Merz, B.: Changes in the flood hazard in Germany through changing frequency and persistence of circulation patterns, Natural Hazards and Earth System Sciences, 9, 1409–1423, https://doi.org/10.5194/nhess-9-1409-2009, 2009.

Pfister, L.: Weather Type Reconstruction using Machine Learning Approaches [data set and code], https://doi.org/10.48350/195666, 2024.

Pfister, L., Hupfer, F., Brugnara, Y., Munz, L., Villiger, L., Meyer, L., Schwander, M., Isotta, F. A., Rohr, C., and Brönnimann, S.: Early instrumental meteorological measurements in Switzerland, Climate of the Past, 15, 1345–1361, https://doi.org/10.5194/cp-15-1345-2019, 2019.

Philipp, A., Bartholy, J., Beck, C., Erpicum, M., Esteban, P., Fettweis, X., Huth, R., James, P., Jourdain, S., Kreienkamp, F., Krennert, T., Lykoudis, S., Michalides, S. C., Pianko-Kluczynska, K., Post, P., Álvarez, D. R., Schiemann, R., Spekat, A., and Tymvios, F. S.: Cost733cat – A database of weather and circulation type classifications, Physics and Chemistry of the Earth, 35, 360–373, https://doi.org/10.1016/j.pce.2009.12.010, 2010.

Philipp, A., Beck, C., Huth, R., and Jacobeit, J.: Development and comparison of circulation type classifications using the COST 733 dataset and software, International Journal of Climatology, 36, 2673–2691, https://doi.org/10.1002/joc.3920, 2016.

Racah, E., Beckham, C., Maharaj, T., Kahou, S. E., Prabhat, and Pal, C.: Extreme weather: a large-scale climate dataset for semi-supervised detection, localization, and understanding of extreme weather events, in: Proceedings of the 31st International Conference on Neural Information Processing Systems, NIPS'17, pp. 3405–3416, Curran Associates Inc., Red Hook, NY, USA, 2017.

Rohrer, M., Croci-Maspoli, M., and Appenzeller, C.: Climate change and circulation types in the Alpine region, Meteorologische Zeitschrift, 26, 83–92, https://doi.org/10.1127/metz/2016/0681, 2017.

Rosenblatt, F.: The perceptron: A probabilistic model for information storage and organization in the brain, Psychological Review, 65, 386–408, https://doi.org/10.1037/h0042519, 1958.

Schiemann, R. and Frei, C.: How to quantify the resolution of surface climate by circulation types: An example for Alpine precipitation, Physics and Chemistry of the Earth, Parts A/B/C, 35, 403–410, https://doi.org/10.1016/j.pce.2009.09.005, 2010.

Schlef, K. E., Moradkhani, H., and Lall, U.: Atmospheric Circulation Patterns Associated with Extreme United States Floods Identified via Machine Learning, Scientific Reports, 9, 7171, https://doi.org/10.1038/s41598-019-43496-w, 2019.

Schwander, M., Brönnimann, S., Delaygue, G., Rohrer, M., Auchmann, R., and Brugnara, Y.: Reconstruction of Central European Daily Weather Types Back to 1763: Reconstruction of Central European Daily Weather Types, International Journal of Climatology, 37, 30–44, https://doi.org/10.1002/joc.4974, 2017.

Schüepp, M.: Witterungsklimatologie. Beiheft zu den Annalen der Schweizerischen Meteorologischen Anstalt. [Climatology of Weather Conditions. Supplement to the Annals of the Swiss Meteorological Office], Tech. Rep. 3, Schweizerische Meteorologische Anstalt, Zurich, Switzerland, 1979.

Slivinski, L. C., Compo, G. P., Whitaker, J. S., Sardeshmukh, P. D., Giese, B. S., McColl, C., Allan, R., Yin, X., Vose, R., Titchner, H., Kennedy, J., Spencer, L. J., Ashcroft, L., Brönnimann, S., Brunet, M., Camuffo, D., Cornes, R., Cram, T. A., Crouthamel, R., Domínguez-Castro, F., Freeman, J. E., Gergis, J., Hawkins, E., Jones, P. D., Jourdain, S., Kaplan, A., Kubota, H., Blancq, F. L., Lee, T., Lorrey, A., Luterbacher, J., Maugeri, M., Mock, C. J., Moore, G. K., Przybylak, R., Pudmenzky, C., Reason, C., Slonosky, V. C., Smith, C. A., Tinz, B., Trewin, B., Valente, M. A., Wang, X. L., Wilkinson, C., Wood, K., and Wyszyński, P.: Towards a more reliable historical reanalysis: Improvements for version 3 of the Twentieth Century Reanalysis system, Quarterly Journal of the Royal Meteorological Society, 145, 2876–2908, https://doi.org/10.1002/qj.3598, 2019.

Snoek, J., Larochelle, H., and Adams, R. P.: Practical Bayesian optimization of machine learning algorithms, in: Proceedings of the 25th International Conference on Neural Information Processing Systems - Volume 2, NIPS'12, pp. 2951–2959, Curran Associates Inc., Red Hook, NY, USA, 2012.

Stepanek, P.: Air Temperature Fluctuations in the Czech Republic in the Period of Instrumental Measurements., PhD Thesis, Masaryk University, Brno, Czech Republic, 2005.

Stryhal, J. and Huth, R.: Classifications of winter atmospheric circulation patterns: validation of CMIP5 GCMs over Europe and the North Atlantic, Climate Dynamics, 52, 3575–3598, https://doi.org/10.1007/s00382-018-4344-7, 2019.

Sýkorová, P. and Huth, R.: The applicability of the Hess–Brezowsky synoptic classification to the description of climate elements in Europe, Theoretical and Applied Climatology, 142, 1295–1309, https://doi.org/10.1007/s00704-020-03375-1, 2020.

Thomas, C., Voulgarakis, A., Lim, G., Haigh, J., and Nowack, P.: An unsupervised learning approach to identifying blocking events: the case of European summer, Weather and Climate Dynamics, 2, 581–608, https://doi.org/10.5194/wcd-2-581-2021, 2021.

Truong, C., Oudre, L., and Vayatis, N.: Selective review of offline change point detection methods, Signal Processing, 167, 107 299, https://doi.org/10.1016/j.sigpro.2019.107299, 2020.

Uppala, S. M., KÅllberg, P. W., Simmons, A. J., Andrae, U., Bechtold, V. D. C., Fiorino, M., Gibson, J. K., Haseler, J., Hernandez, A., Kelly, G. A., Li, X., Onogi, K., Saarinen, S., Sokka, N., Allan, R. P., Andersson, E., Arpe, K., Balmaseda, M. A., Beljaars, A. C. M., Berg, L. V. D., Bidlot, J., Bormann, N., Caires, S., Chevallier, F., Dethof, A., Dragosavac, M., Fisher, M., Fuentes, M., Hagemann, S., Hólm, E., Hoskins, B. J., Isaksen, L., Janssen, P. A. E. M., Jenne, R., Mcnally, A. P., Mahfouf, J., Morcrette, J., Rayner, N. A., Saunders, R. W., Simon, P., Sterl, A., Trenberth, K. E., Untch, A., Vasiljevic, D., Viterbo, P., and Woollen, J.: The ERA-40 re-analysis, Quarterly Journal of the Royal Meteorological Society, 131, 2961–3012, https://doi.org/10.1256/qj.04.176, 2005.

Valler, V., Franke, J., Brugnara, Y., and Brönnimann, S.: An updated global atmospheric paleo-reanalysis covering the last 400 years, Geoscience Data Journal, 9, 89–107, https://doi.org/10.1002/gdj3.121, 2022.

Wang, X., Sun, Y., Luo, D., and Peng, J.: Comparative study of machine learning approaches for predicting short-term photovoltaic power output based on weather type classification, Energy, 240, 122 733, https://doi.org/10.1016/j.energy.2021.122733, 2022.

Wang, X. L.: Penalized Maximal F Test for Detecting Undocumented Mean Shift without Trend Change, Journal of Atmospheric and Oceanic Technology, 25, 368–384, https://doi.org/10.1175/2007JTECHA982.1, 2008.

Wang, X. L. and Feng, Y.: RHtestsV4 [code], https://github.com/ECCC-CDAS/RHtests, 2018.

Wang, X. L., Wen, Q. H., and Wu, Y.: Penalized Maximal t Test for Detecting Undocumented Mean Change in Climate Data Series, Journal of Applied Meteorology and Climatology, 46, 916–931, https://doi.org/10.1175/JAM2504.1, 2007.

Wanner, H., Gyalistras, D., Luterbacher, J., Rickli, R., Salvisberg, E., and Schmutz, C., eds.: Klimawandel im Schweizer Alpenraum, Vdf Hochschulverlag, Zurich, Switzerland, 1st edn., 2000.

Weusthoff, T.: Weather Type Classification at MeteoSwiss, Tech. Rep. 235, MeteoSwiss, Zurich, Switzerland, 2011.

Williams, J. K., Ahijevych, D. A., Kessinger, C. J., Saxen, T. R., Steiner, M., and Dettling, S.: A Machine Learning Approach to Finding Weather Regimes and Skillful Predictor Combinations for Short-Term Storm Forecasting, in: 13th Conference on Aviation, Range and Aerospace Meteorology, New Orleans, LA, USA, http://n2t.net/ark:/85065/d7rb73p8, 2008.

Winkler, P.: Hohenpeissnberg 1781-2006: das älteste Bergobservatorium der Welt [Hohenpeissenberg 1781-2006: the oldest Mountain Observatory in the World], no. 7 in Geschichte der Meteorologie in Deutschland, Deutscher Wetterdienst, Offenbach am Main, Germany, 2006.

Winkler, P.: Revision and necessary correction of the long-term temperature series of Hohenpeissenberg, 1781–2006, Theoretical and Applied Climatology, 98, 259–268, https://doi.org/10.1007/s00704-009-0108-y, 2009.